

Spatiotemporal variability in phytoplankton size class modulated by summer monsoon wind forcing in the central Arabian Sea

Mintu Chowdhury^{1,#}, Haimanti Biswas^{1,*}, Saumya Silori^{1,\$}, Diksha Sharma^{1,\$\$}

¹CSIR National Institute of Oceanography, Biological Oceanography Division,
Dona Paula, Goa 403004, India.

#Current affiliation: Centre for Marine Living Resources and Ecology,
Ministry of Earth Sciences, Kochi, Kerala 682508, India.

\$Current affiliation: Royal Belgian Institute of Natural Sciences,
Vautierstreet, 29, 1000 Brussels, Belgium.

\$\$Current affiliation: Department of Earth Science, Dartmouth College,
Hanover, NH 03755, United States.

*Corresponding author: haimanti.biswas@nio.org; haimanti.biswas.nio@gmail.com

Abstract

The Arabian Sea is an area of intense ocean-atmospheric coupling that impacts its physicochemical, and biological processes. During the summer monsoon (June –September), in the central Arabian Sea, a low-level atmospheric jet blows parallel to the Arabian Peninsula causing open ocean upwelling in the north and downwelling in the south of the jet axis. High wind speeds are witnessed in the jet axis which advect nutrients from the Somali coast. Consequently, hydrography and physicochemical parameters show high spatial variability. In this dynamic region, phytoplankton size class distribution, directly controlled by nutrient supply, can be modulated by monsoon wind variability via upwelling, advection, and entrainment, however, has not been investigated recently. We studied phytoplankton size class related to atmospheric forcing, hydrography, and nutrient stoichiometry in August 2017 and 2018 along 64° E (11° N–21° N). Chemical taxonomy-based analysis (CHEMTAX and manual) revealed that in the north, upwelling-driven nutrient enrichment supported microphytoplankton, mostly diatoms contributing ~50% to phytoplankton biomass. A stronger upwelling due to higher wind forcing in 2018 compared to 2017 resulted in an enhanced nutrient supply as well as an increased contribution of diatoms. Prymnesiophytic nanophytoplankton distribution was linked to mixed layer depths with insignificant spatial variability (20–30%). Conversely, in the nutrient-poor southern region, zeaxanthin and DV-Chla containing picocyanobacteria and prochlorophytes contributed >50% to the total phytoplankton biomass and were associated with high temperatures. Likely, increasing warming and related changes in monsoon intensity might directly influence phytoplankton size classes impacting trophic transfer and carbon cycling.

Keywords: Phytoplankton pigments; Central Arabian Sea; Summer monsoon; Diatoms; Cyanobacteria; Carbon flux

Key Points

- Marker pigment-based phytoplankton community and size classes were analyzed during the summer monsoon (2017-2018) in the central Arabian Sea
- Phytoplankton community and size classes were mostly governed by hydrography and nutrient stoichiometry induced by monsoon wind forcing
- Any future change in monsoon strength could impact phytoplankton size classes and can be cascaded to trophic transfer and carbon export

Plain language summary

The Arabian Sea, a part of the North Indian Ocean, is an area of strong ocean-atmospheric coupling and high biological productivity. This basin provides livelihood to the surrounding countries; however, the increasing rate of sea surface temperature raises our concern about the subsequent changes in ecosystem services. During the summer monsoon, high biological productivity occurs at certain locations due to upwelling when nutrients are added to the surface by physical forcing. In this study, we have described the results from two cruises (August 2017 & 2018) along the central Arabian Sea that experiences open ocean upwelling in its northern flank and downwelling in the south during the summer monsoon. Atmospheric forcing was found to directly control the hydrography, nutrient availability, and phytoplankton size class distribution across the central Arabian Sea with a distinct interannual difference. The phytoplankton size classes (micro, nano, and picophytoplankton) constructed using the marker pigment data showed prominent spatial and interannual variability that was consistent with the microscopic study. Any future change in the strength and onset of monsoon or increase in sea surface temperature may directly impact nutrient distribution that can be cascaded to the phytoplankton community, higher trophic level, and carbon export flux.

Introduction

In the global ocean, nearly 40 -50 Pg C per year is removed by marine phytoplankton alone via oxygenic photosynthesis (Field et al. 1998; Falkowski and Raven 2013). A small fraction of this organic matter eventually sinks to the deep sea and is stored for centuries to millennia (Boyd and Trull 2007) (Marine Biological Carbon Pump) and plays a key role in buffering our climate. Trophic transfer and downward export of phytodetritus to the deep sea can be directly dependent on the phytoplankton community and cell size (Legendre and Lefevre 1989; Hansen et al. 1994; Jennings et al. 2002). Phytoplankton cell size controls their resource utilization efficiency, growth, metabolism, and their niche occupancy (Chisholm 1992; Lichtman and Klausmeier 2008). The availability of the major dissolved inorganic nutrients i.e. nitrogen, phosphorus, and silicon as well as their ratios are the key factors in regulating marine phytoplankton cell size, growth, community structure, and distribution (Margalef 1978; Aksnes and Egge 1991; Edwards and Richardson 2004; Klausmeier et al. 2008). In addition to light and temperature, trace metals like iron also play a major role in phytoplankton growth (Martin et al. 1990; Twining and Baines 2013). Phytoplankton can be categorized based on their size as microphytoplankton (20–200 μm), nanophytoplankton (2–20 μm), and picophytoplankton (0.2–2 μm) (Sieburth et al. 1978). Diatoms and dinoflagellates are the dominant components of marine microphytoplankton; whereas coccolithophores and picocyanobacteria belong to nano and picophytoplankton, respectively (Falkowski and Knoll 2011). Nutrient uptake efficiency of cells inversely varies with cell size and hence smaller phytoplankton are more efficient in consuming nutrients even in oligotrophic waters (Marañón et al. 2012).

The Arabian Sea, one of the highest productive regions in the global ocean, is under the direct influence of the Indian monsoon system. This basin shows high seasonality in its physical processes due to the reversal of the monsoon winds (Ramage 1987). During the summer months, the Asian landmass warms up and creates a strong low-pressure zone. Consequently, the Southwesterly monsoon wind develops and blows over the Arabian Sea causing strong upwelling in the coast of Somalia and Oman as well as in the southwest coast of India. At the same time, the monsoon winds also develop a low-level atmospheric jet (Findlater Jet, Findlater 1969) blowing perpendicular to the coast of the Arabian Peninsula causing open ocean upwelling in the northern part of the jet. Therefore, the strong ocean-atmospheric interaction at this region directly influences the mixed layer depth (MLD) as well as nutrient supply to the euphotic layers. Consequently, the nutrient-rich upwelled waters support intense phytoplankton blooms, dominated by diatoms that can be either grazed (trophic transfer) and/or exported vertically (Landry et al. 1998; Latasa and Bidigare 1998; Tarran et al. 1999; Brown et al. 2002; Rixen et al. 2019; Chowdhury et al. 2021). A direct correlation was derived between surface processes and deeper waters by linking surface productivity, particle flux, and the strength of the summer monsoon which is characterized by wind speeds, sea surface temperature (SST), and upwelling (Haake et al. 1993; Rixen et al. 1996). The relative contribution of phytoplankton to organic matter varies seasonally in the Arabian Sea and may directly influence the export flux potential (Gauns et al. 2005). High productivity due to the monsoonal forcing and poor ventilation of the mesopelagic waters in the Arabian Sea result in the formation of one of the most prominent oxygen minimum zones (OMZs) (occurs between 150–1000 m depth) (Banse et al. 2014; Rixen et al. 2020). Nevertheless, the places of high productivity and the OMZs are decoupled in this region (Zhang et al. 2022).

In the context of climate change, the projected warming coupled with stratification may have a direct influence on the phytoplankton size and community composition (Rousseaux and Gregg 2015). Particularly, the rapid warming of the Arabian Sea is raising concern (Sharma et al. 2023) as it may change the nutrient supply to phytoplankton, and consequent modifications in trophic transfer and carbon export to the deep sea. A few studies, conducted during the winter monsoon proposed a complete regime shift from diatoms to mixotrophic dinoflagellates (Goes and Gomes 2016; Xiang et al. 2019). A further intensification of such events has been projected (Lotliker et al. 2018) due to rapid warming, stratification (Prasannakumar et al. 2009), and changes in the monsoon wind intensity (Roxy 2017). Chowdhury et al. (2021) analyzed the phytoplankton by microscopy in two summer monsoon cruises (Aug 2017 and 2018) along the central Arabian Sea showing that diatoms dominated the phytoplankton community, especially in the upwelling region and along the jet axis. On the other hand, smaller diatoms and dinoflagellates occupied the southern region which experiences downwelling and

low nutrients. This trend was consistent with earlier JGOFS reports. Interestingly, despite the decreasing contribution of microphytoplankton southward, particulate organic carbon (POC) contents were comparable (Silori et al. 2021) hinting at the possibility of the contribution of smaller phytoplankton to the POC pool. Nevertheless, using microscopy (Utermöhl 1958) estimating the contributions of smaller size classes (nano and pico) to phytoplankton biomass remained inconclusive and needs specialized methods like marker pigment-based analysis (Wright and Jeffrey 2006) or flow cytometry. Phytoplankton marker pigment analysis by High-Performance Liquid Chromatography (HPLC) has now been extensively used to determine phytoplankton size classes (Claustre 1994; Vidussi et al. 2001; Uitz et al. 2006). The pigment-based community analysis in the western and central Arabian Sea has been studied during the Joint Global Ocean Flux Study (JGOFS) in the 1990s (Latasa and Bidigare 1998; Barlow et al. 1999; Brown et al. 2002; Goericke 2002). In recent years, systematic studies targeting phytoplankton size class analysis related to summer monsoon wind forcing have rarely been investigated. Thus in this study, we have tried to answer two key questions 1) how nutrient dynamics impacted the relative contributions of different size classes of phytoplankton to total biomass during 2017 -2018? 2) how did phytoplankton size class distribution vary spatially (north to south) with changing monsoon wind forcing? The possible implications of such spatiotemporal variability in phytoplankton size classes related to phytodetritus flux have also been discussed.

Material and methods

Surface wind data

Monthly-averaged reanalysis wind data with a resolution of $1^\circ \times 1^\circ$ were obtained from the National Centre for Environmental Prediction (NCEP), Maryland, USA, an open-access library for the entire study region (Kalnay et al. 1996).

Sample collection

Two cruises were undertaken during the summer monsoon onboard *RV Sindhu Sadhana* from Aug 3 to 28, 2017 (SSD 040) and from Aug 2 to 31, 2018 (SSD 055). Water samples were collected from 11 locations in the central Arabian Sea (along 64°E) from 21°N to 11°N at an interval of 1° . Due to extreme weather conditions, the 17°N station in 2017 was not sampled. Water samples for bulk parameters were collected down to 120 m depth using a Niskin sampler (24 bottles, 10 L) mounted on a rosette frame carrying a CTD (Sea-Bird, USA) system. However, for phytoplankton pigment analyses, water samples were collected up to 60 m (surface, 5, 10, 20, 30, 40, 50, and 60 m) based on the fluorescence signals obtained from CTD sensors. The values of depths, sea surface salinity (SSS), sea surface temperature (SST), and dissolved oxygen (DO) were derived from pre-calibrated sensors

fitted to the CTD. The MLD was calculated using a 0.2 kg m^{-3} density difference from the surface (Levitus 1982). Due to some technical reasons, the PAR data was not possible to retrieve properly and hence missing from this study.

Dissolved inorganic nutrient analyses

The major dissolved inorganic nutrients were measured by spectrophotometric methods against known standard-based calibration. The concentrations of nitrate+nitrite and dissolved silicate (DSi) were analyzed in duplicate manually on board immediately after the collection following the standard colourimetric method (UV-1800 UV-Vis Spectrophotometer, Shimadzu) by Grasshoff et al. (2009) against the standard reference solutions (KNO_3 , and Na_2SiF_6). Dissolved inorganic phosphate (DIP) was analyzed by Knap et al. (1996) (UNESCO method) using the reference solution K_2HPO_4 . Each of these methods has been calibrated with certified standard reference material (Merck). The precision ranged from 96% to 98% for measurements of DIP, DSi, nitrate+nitrite, and nitrite ($1 \text{ }\mu\text{M}$), with standard deviations between 0.02 and $0.1 \text{ }\mu\text{M}$. Please note that ammonium was not analyzed due to some technical issues onboard. It should be noted that physicochemical parameters were published in our previous work (Chowdhury et al. 2021, Silori et al. 2021).

Phytoplankton pigment analysis by HPLC

For analyzing phytopigment, 1.5 L seawater was collected in an amber-colored bottle, and soon after the collection, seawater samples were filtered onto GF/F filters (25 mm, Whatman) in a temperature-controlled dimly lit room using a vacuum pump (Millipore) keeping the pressure under 200 Mb for phytoplankton pigment analysis. Amber-colored polycarbonate filtration cups were used to minimize light exposure. After the filtration, the filters were folded in quarters and wrapped with aluminum foil, and stored at -80°C until further analysis in the shore laboratory. Pigment samples were extracted by soaking the filter paper in 3 mL ice-cold 100% methanol (HPLC grade, Merck chemicals) overnight (18–20 hr.) at -20°C . A tissue homogenizer (Ultra Turrax, Germany) was used to break the cells keeping the bottles on an ice-filled tray followed by a filtration using a Teflon syringe cartridge (pore size $0.45 \text{ }\mu\text{m}$) to remove the cellular debris. These filtrates with pigment extracts were mixed with a buffer composed of 28 mM aqueous tetra butyl ammonium acetate (TBAA; AR Grade, TCI) at pH 6.5 and methanol in a 9:1 ratio. The HPLC system (Shimadzu Prominence i-Series) was used to quantify the phytoplankton pigments following the method of Van Heukelem and Thomas (2001). The HPLC equipped with a Shim Pack GIST C8 column [4.6 mm (diameter) \times 150 mm (length); pore size $3.0 \text{ }\mu\text{m}$] was used to separate the pigments and a photodiode array (PDA) detector for detection of pigments. Individual pigments were identified using the standard pigments procured from DHI (Denmark). A

methanol-based reversed-phase linear gradient solvent system (binary gradient elution using solvent A: 70:30 methanol: 28 mM TBAA at pH 6.5, solvent B: methanol; linear gradient from 5 to 95% solvent B in 22 min, an isocratic hold of 95% solvent B till 29 min) was applied. The solvent flow rate of 1.1 mL min⁻¹ was maintained and 500 µL of the sample was taken as the injection volume. The quantification of the marker pigment was done based on the peak area of the standard pigments.

Phytoplankton size classes were obtained using the marker pigments detected in HPLC analysis. The weighted sum of the seven major diagnostic pigments [Fucoxanthin (Fuco), peridinin (Perid), 19'-hexanoyloxyfucoxanthin (19'HF), 19'-butanoyloxyfucoxanthin (19'BF), alloxanthin (Allo), chlorophyll b (Chlb), and zeaxanthin (Zea)] have been used to estimate the biomass associated with three pigment-derived size classes, i.e., microphytoplankton (20–200 µm), nanophytoplankton (2–20 µm), and picophytoplankton (0.2 –2 µm) as proposed by Uitz et al. 2006 (Supplementary Table S1). For calculating the sum of all weighted diagnostic pigments (ΣDPw) the following formula was used:

$$\Sigma DPw = 1.41[\text{Fuco}] + 1.1[\text{Perid}] + 1.27[19'\text{HF}] + 0.35 [19'\text{BF}] + 0.60[\text{Allo}] + 1.01 [\text{Chlb}] + 0.86 [\text{Zea}]$$

The fractions of the chlorophyll-*a* concentration associated with each of the three phytoplankton classes were then derived according to the following ratios (Vidussi et al. 2001).

$$\text{Micro (\%)} = [(1.41[\text{Fuco}] + 1.1[\text{Perid}]) / \Sigma DPw] * 100$$

$$\text{Nano (\%)} = [(1.27[19'\text{HF}] + 0.35 [19'\text{BF}] + 0.60[\text{Allo}]) / \Sigma DPw] * 100$$

$$\text{Pico (\%)} = [(1.01 [\text{Chlb}] + 0.86 [\text{Zea}]) / \Sigma DPw] * 100$$

Analysis with CHEMTAX

Chemical taxonomy software (CHEMTAX, version 1.95) was used to calculate the relative contribution of individual phytoplankton groups to total phytoplankton biomass (TChl_a) (Mackey et al., 1996, Wright et al., 1996, Wright et al., 2009, Wright et al., 2010). Please note that DV-Chl_a was added to Chl_a to get total phytoplankton biomass (TChl_a). As input values, the initial pigment ratios specific to the Arabian Sea (Roy et al. 2015) were used because this software is sensitive to initial ratio matrix input values. A more detailed methodology can be found in Mackey et al. (1996). In total, 7 phytoplankton groups (prasinophytes, prochlorophytes, dinoflagellates, prymnesiophytes, chlorophytes, cyanobacteria, and diatoms) were used in CHEMTAX analysis. The following pigments were considered for this analysis: divinyl chlorophyll *a*, zeaxanthin, chlorophyll *b*, and chlorophyll *a*, peridinin, 19'-butanoyloxyfucoxanthin, fucoxanthin, 19'-hexanoyloxyfucoxanthin, prasinoxanthin. The pigment ratios after optimization (initial and final) are provided in Supplementary Table S2.

Univariate and multivariate analysis

The correlation between the major marker pigments and total Chlorophyll *a* (Chl *a*+DV-Chl*a*) has been plotted in Microsoft Excel 2016. For multivariate analysis, environmental and biological parameters up to 60 m deep were used. To compute correlations matrices between environmental variables (wind speed, salinity, temperature, DO, MLD, NO₂+NO₃, DIP, DSi, Si:N, N:P and major phytoplankton components (size class and diagnostic pigments) at significance level $p \leq 0.05$, PAST v4.03 (Hammer et al. 2001) has been used. The CANOCO version 4.5 software was used to study the relationships between biotic factors (phytoplankton class and their ratio) and some environmental variables (Ter Braak & Šmilauer 2002). Detrended Correspondence Analysis (DCA) was used to analyze the data to determine the best ordination method, and the results showed that the axis gradient length was < 2 . RDA, a linear multivariate model, was utilized to explain the association between environmental and biological variables (Leps and Šmilauer, 2003). The RDA employed Monte Carlo simulation to examine the levels of significance of environmental variables and biotic components.

Results

Physicochemical variability

Based on the windspeed data, MLD, and Ekman pumping velocities, the cruise transect (Fig. 1) (21° N, 64°E and 11°N, 64°E) was divided into three regions 1) the north of the Findlater Jet (NFJ; 21°–19° N), 2) the axis of the Findlater Jet (AFJ; 18–16° N) and 3) the south of the Findlater Jet (SFJ; 15–11° N). The satellite-based wind speed data showed lower values in 2017 (Fig. 1A) than in 2018 (Fig. 1B). The maximum wind speed was noticed in the AFJ with the highest value at 18° N during both years. The shallowest MLD persisted in the NFJ and increased towards the south without any noticeable variability in the NFJ (Fig. 1C). However, a noticeable difference was observed in the SFJ where the maximum MLD (110 m) was recorded at 15° N during 2017 and 13° N (137 m) during 2018.

Latitudinal variations of water temperature (Fig. 2A, 2B) covaried with the wind speeds and MLDs, with substantially low SST during 2018. This was evident from low SST in the NFJ as well as in the AFJ ($26.2 \pm 0.3^\circ\text{C}$) in 2018 (Fig. Supplementary 1). The D₂₄ (24° C isotherm) was found at much shallower depths in the NFJ and deepened towards the south. However, in 2018, the presence of D₂₄ was found at shallower depths in the NFJ than in 2017. The salinity values (Fig. 2C, 2D; Table 1) did not show any significant variability (36.20–36.55 PSU in 2017 and 36.36–36.63 PSU in 2018). The isohaline nature of the water column is confined to the upper 60 m depth. DO concentrations ranged from 4.1–4.5 mL L⁻¹ (4.3 ± 0.5 mL L⁻¹) and 3.8–4.2 mL L⁻¹ (av. 4.0 ± 0.4 mL L⁻¹) during 2017 and 2018,

respectively (Fig. 2E, 2F). The 2.5 mL L⁻¹ isoline coincided with the D₂₄ isotherm in the NFJ at 60 m depth during 2017 but it was found at a shallower depth (~50 m) during 2018 along with the isotherm.

Nutrient stoichiometry

The distribution of dissolved inorganic nutrients covaried with MLDs and showed significant variation from north to south as well from 2017 to 2018. The nutricline depth varied between 40–60 m and was confined within 20–21° N with considerably higher concentration in 2018. The nutricline depth started increasing from 19° N to further south where it was recorded within 100–120 m depth. Nitrate+nitrite concentrations (Fig. 3A, 3B) ranged between 0.01 to 2.42 μmol L⁻¹ and 2.17–5.65 μmol L⁻¹ above the nutricline in the NFJ in 2017 and 2018, respectively. In 2018, the values of nitrate+nitrite, DIP (Fig. 3C, 3D), and DSi (Fig. 3E, 3F) were significantly higher ($p < 0.05$) than in 2017. The surface concentrations of DIP and DSi in 2017, ranged between 0.4–1.2 μmol L⁻¹, and 0.4–2.0 μmol L⁻¹, respectively. Whereas, in 2018, DIP and DSi varied between 0.2–2.2 μmol L⁻¹. And 0.16–2.48 μmol L⁻¹, respectively. The maximum value of DSi in 2017 was found (1.74±0.61 μmol L⁻¹) in the AFJ, but in 2018 the highest value (2.92±0.96 μmol L⁻¹) was noticed in the SFJ and was very low in the NFJ (0.92±1.37). Si: N ratio showed significant ($p < 0.05$) variability (Fig. 3G, 3H) from 2017 to 2018. In 2017, the Si:N ratio was higher (16.2) in the NFJ and decreased substantially (<3) in 2018. In the AFJ, the ratio remained less than 1. A three-times higher value was observed in the south in 2017 (2.51±2.93) than in 2018 (0.80±0.33). N:P ratios (Nitrate+nitrite: DIP) showed higher values in 2018 (5.2±2.3) compared to 2017 (3.7±3.4) (Fig. 3I, 3J). These ratios, however, were lower than the Redfield ratio (16:1). The lowest value was recorded from the NFJ (1.04±0.16) above the thermocline during 2017, and almost 4 times higher values were seen in the AFJ and SFJ.

Pigment distribution

Other than chlorophyll-*a* (Chl*a*) and divinyl chlorophyll a+b (DV-Chl*a*), pigment analysis revealed the presence of fucoxanthin, 19'-hexanoyloxyfucoxanthin, 19'-butanoyloxyfucoxanthin, zeaxanthin, chlorophyll *b*, peridinin Chlorophyll *c*₁+*c*₂ (Chl*c*₂), chlorophyll *c*₃ (Chl*c*₃), diadinoxanthin (DD), β-carotene, and diatoxanthin (DT) (Supplementary Table S1). Prasinoxanthin, violaxanthin, 9-cis-Neoxanthin, alloxanthin, and pheophorbide-*a* were noticed at various depths occasionally at a few stations.

TChl*a* (sum of Chl*a* + DV-Chl*a*) concentration (Fig. 4A, 4B) in the central Arabian Sea ranged between 0.038 μg L⁻¹ and 0.603 μg L⁻¹ (av. 0.30±0.15 μg L⁻¹) in 2017 and 0.12–0.651 μg L⁻¹ (av. 0.30±0.12 μg L⁻¹) in 2018. The maximum concentration was observed at 18°N (2017) and 19°N (2018) at the surface. In 2017 high TChl*a* concentration (0.46±0.06 μg L⁻¹) was recorded at 21°N (0–

40 m); however, while moving southward (18° N – 14° N) such high values (av. 0.54±0.05 µg L⁻¹) was mostly confined within 0–20 m depth except at 15°N (av. 0.32±0.02 µg L⁻¹) (Fig. 4A). In 2018, a high TChla value was noticed till 20 m (av. 0.43±0.10 µg L⁻¹) from the NFJ to AFJ except at 18°N (av. 0.21±0.03 µg L⁻¹) (Fig. 4B). DV-Chla (Fig. 4C, 4D) concentrations did not vary significantly (Table 1) except at 18° N, 14° N (2017), and 21° N (2018) where relatively higher values were noticed. The concentrations of Fuco (Fig. 4E, 4F) in 2018 were mostly dominated towards the NFJ, particularly between 20–21° N at 0–40 m depths (av. 0.13±0.04 µg L⁻¹); on the contrary in 2017, Fuco dominance (av. 0.15±0.03 µg L⁻¹) was limited only to 21°N. Its concentration was reduced sharply towards the SFJ and exhibited a homogenous vertical distribution in the southern stations. Perid concentrations (Fig. 4G, 4H) were higher in 2017 than in 2018, with the maximum value at 20° N in both years and a few higher values between 14° and 18° N. The maximum concentration of 19'HF was found at 18°N (0.073 µg L⁻¹) at the surface and 13°N (0.066 µg L⁻¹) at 40 m during 2017 and 2018 respectively. The highest concentration of 19'HF was confined within 40 m water depth between 13°N and 18°N (2017) and from 12°N–16°N (2018) (Fig. 5A, 5B) with less variability between the years (Table 1). The lowest 19'HF concentration was observed at the NFJ (21°N and 20°N) for both years. 19'BF (Fig. 5C, 5D) followed a similar distribution pattern like 19'HF, especially at the central stations. 19'BF showed high concentration at 15°N (0.025 µg L⁻¹) at 40 m in 2017 and at 21°N (0.034 µg L⁻¹) at 20 m in 2018. The concentrations of Zea (Fig. 5E, 5F) revealed significant spatiotemporal variability (Table 1). Zea was largely dominated in the SFJ between 0–20 m. The values ranged between 0.001–0.181 µg L⁻¹ and 0.001–0.095 µg L⁻¹ during 2017 and 2018, respectively. The maximum concentration was recorded at 13°N and the average value was higher in 2017 (av. 0.046±0.045 µg L⁻¹) than in 2018 (av. 0.030±0.023 µg L⁻¹). The concentrations of Chlb (Fig. 5G) ranged between 0.005–0.110 (av. 0.046±0.028 µg L⁻¹) with high concentrations at four stations (12°, 14°, 18°, and 20°N) in 2017. Whereas in 2018, Chlb concentration (Fig. 5H) ranged between 0.003–0.171 (av. 0.048±0.028 µg L⁻¹) with notable high values at station 13°N, 17°N, and 19°N. The distribution of some accessory pigments such as Chlorophyllc₂, Chlorophyllc₃, Diadinoxanthin, and β-carotene was shown in Supplementary Fig. S2.

Correlations among different pigments

Fuco and TChla concentrations varied linearly ($p < 0.01$) in the NFJ and AFJ in 2017, but were insignificant in the NFZ in 2018 as well as in the SFJ during both years ($p > 0.05$) (Supplementary Table S3, Supplementary Fig. S3, S4). Importantly, the slope of the equation in the NFZ was ≈ 0.21 representing the average ratio of Fuco/Chla and decreased more than three times in the AFJ and SFJ.

Perid and TChla concentrations were also linearly correlated ($p < 0.05$) in the AFJ, however, became insignificant in the NFJ (Supplementary Table S3). ^{19}HF and TChla levels showed significant positive correlations ($p < 0.05$) in all stations during both years. However, the slope of the equation (representing the ratio of $^{19}\text{HF}/\text{TChla}$) was 0.041 in the NFJ and doubled in the AFJ. The slope of the linear correlation between Zea and TChla levels was 0.077 in the NFJ and AFJ, but was enhanced by more than 2.5 times in the SFJ. DV-Chla and TChla concentrations showed high linearity (positive) and the slope value was nearly 0.06 throughout both years along the transect.

Contribution of individual groups to total phytoplankton biomass

CHEMTAX analysis revealed that among the total 7 groups (Fig. 6) of phytoplankton contributing to Chla, diatoms (Fig. 6A, 6B) were prominent mostly towards the NFJ (50-60%) where the upwelling impact was the highest. Their contributions to total Chla were moderate along AFJ (6-9%) and reached minimum values at the SFJ. Within the sampling years, the contribution of diatoms was higher (~40%) in 2018 compared to 2017. The next abundant group was dinoflagellate (Fig. 6C, 6D), which revealed a similar spatial distribution pattern as diatoms. However, their abundance was higher in 2017 than in 2018. Prymnesiophytes were mostly found along the AFJ during both years with relatively higher values in 2017 (Fig. 6E) compared to 2018 (Fig. 6F). Contrary to the first two groups, this phytoplankton group was found throughout the water column including the deeper depths. In the SFJ, the contributions of cyanobacteria (Fig. 6G, 6H) were remarkably higher (~40%) than the NFJ (5-7%) and AFJ (12%). Prochlorophytes were quite low and homogeneously distributed except a patchy distribution was found at the AFJ in 2017 (Fig. 6I), but was absent in 2018 (Fig. 6J). The contribution of prasinophytes (Supplementary Fig. S5A, S5B) was quite lower than other groups. Their relative contribution was mostly confined to the AFJ compared to the NFJ and SFJ. The relative contributions of chlorophytes (Supplementary Fig. S5C, S5D) were very low in the upwelling-dominated region and increased in AFJ and SFJ.

Size class distribution

In addition to the manual calculation [following Uitz et al. (2006) and Vidussi et al. (2001)] the contributions of different phytoplankton size classes to total phytoplankton biomass were also derived using CHEMTAX software. Significant linear correlations were found for micro ($R^2 = 0.833$; $p < 0.00001$), pico ($R^2 = 0.856$; $p < 0.00001$) and nano ($R^2 = 0.569$; $p < 0.00001$) plankton (Fig. 7).

Marker pigment-based size class categorization revealed that microphytoplankton contribution was substantially higher in 2018 than in 2017, particularly in the NFJ (Fig. 8A, 8B). Microphytoplankton contributed almost 70% to TChla at 21°N and 20°N in 2018 (0–40 m)(Fig. 8A, 8B). While moving to

the south, the contribution decreased sharply and reached a minimum value (12%) at 11° N. In 2017, the maximum contribution (72%) of microphytoplankton was restricted to 21°N (Fig. 8A) and decreased southward showing its minimum value (8%) at 12°N. Unlike microphytoplankton, the nanophytoplankton and picophytoplankton were dominant in the southern stations and also contributed more to TChla in 2017 than in 2018 (Fig. 8C- 8F). During both years, nanophytoplankton contributed nearly 30% to TChla from 19°N to 11°N. The highest abundance was found at 12°N (41%) during 2018 and the lowest at 21°N (12%) (Fig. 8C, 8D). Interestingly, nanophytoplankton contribution increased with increasing water depth and contributed nearly 20% to TChla within 0–20 m depth and doubled (35%) at 40–60 m during 2017. Picophytoplankton dominance was observed in the SFJ in both years (Fig. 8E, 8F); the contribution reached up to 68.4% (12°N; 2017) and 53.1% (15°N; 2018). The minimum contribution (15%) of this group was found at the northernmost station (21°N) during both years (Fig. 8E, 8F).

Statistical analysis

The Pearson correlation matrix during 2017 (Fig. 9A) revealed that the water temperature was negatively correlated with the concentrations of NO₂+NO₃, DIP, and microphytoplankton and positively correlated with picophytoplankton. Among dissolved inorganic nutrients, the concentrations of NO₂+NO₃ were positively correlated with microphytoplankton and negatively correlated with picophytoplankton relative contributions. In 2018 (Fig. 9B), NO₂+NO₃ levels were found to be negatively correlated with temperature values, but no significant correlation was found between temperature and phytoplankton size class.

To evaluate the association between the major phytoplankton size classes and physicochemical parameters, a Redundancy Analysis (RDA) was conducted for the values from 2017 (Fig. 9C) and 2018 (Fig. 9D). In 2017, the first two RDA axes of the bi-plot explained 99.1% variability. Axis 1 displayed 65.2% of the total variance and temperature, the concentrations of DO, NO₂+NO₃, DIP, and the ratio of Si:N were associated with this axis. Axis 2 explained 33.9% of the variation and was mainly influenced by MLDs. TChla concentrations, microphytoplankton contribution, and the contribution of diatoms were grouped and influenced by all nutrients. Nanophytoplankton was clustered with MLDs. Picophytoplankton contribution was located opposite to all nutrients and inclined with temperature suggesting their association with oligotrophic warm waters (Fig. 9C). In the RDA plot of 2018 (Fig. 9D), the first two axes explained a 98.2% relationship between phytoplankton components and environmental variables. The concentrations of DO, NO₂+NO₃, the ratio of Si:N and MLDs were correlated with Axis 1. Axis 2 was influenced by DSi and DIP concentrations. TChla contents, the contributions of microphytoplankton, cell abundance, and diatoms, were grouped but influenced by

only NO₂+NO₃ levels in 2018. The contribution of nanophytoplankton, MLD, the concentrations of DSi, and the ratio of Si:N were clustered. Like in 2017, here also picophytoplankton as well as cyanobacterial contribution was found on the opposite axis from the nutrients. The contributions of other groups like nanophytoplankton, prasinophytes, and chlorophytes were linked to MLDs in 2017, and this relation became weaker in 2018.

Discussion

The two-year observation depicted differences in monsoon wind strength that impacted all biogeochemical parameters. The NFJ experiences Ekman suction (Bauer et al. 1991) leading to open-ocean upwelling that uplifts cold nutrient-rich water from the subsurface to the surface (Lee et al. 2000; PrasannaKumar et al. 2001; Brown et al. 2002; Lévy et al. 2007; Liao et al. 2016). The increased wind speed in 2018 was likely to strengthen the Ekman suction process in the NFJ and consequently, a stronger upwelling signature was noticed. The appearance of 21°C isotherm at deeper depths in 2017 compared to 2018 was consistent with this view. Likewise, low oxygenated water (2 mL L⁻¹) was confined to a much shallower depth (40–50 m) in 2018, relative to 2017 (60–70 m). The nutricline was shallower in 2018 compared to 2017, particularly in the NFJ. The lateral advection of nitrate-rich upwelled waters from the Omani Coast also supplements nutrients to the northern region of the central Arabian Sea (Young and Kindle 1994; Kawamiya 2001). Satellite-derived SST profiles indicated the signatures of cooler surface waters advected from the Somali and Oman coasts to the central Arabian Sea were stronger in 2018 (AFJ and NFJ) than in 2017 (only up to AFJ) (Silori et al. 2021). The spatiotemporal difference in phytoplankton size class distribution was directly modulated by these factors and is discussed in the following sections.

A clear shift in phytoplankton size classes from north to south related to physicochemical variability was documented. The NFJ was highest impacted by upwelling-induced nutrient supply and supported high phytoplankton biomass (Garrison et al. 1998; Sawant and Madhupratap 1996; Tarran et al. 1999). Specifically, at 20–21° N, >50% of the total phytoplankton population was contributed by microphytoplankton dominated by diatoms. The contribution of microphytoplankton was higher (in all stations) in the NFJ in 2018 compared to 2017 and can be attributed to enhanced nutrient addition by a stronger upwelling. The shallow MLDs and upwelled water rich in DSi and NO₂+NO₃ mostly supported large diatom growth. The negative correlation between water temperature and nitrate+nitrite levels also strengthened this fact. Nitrate is the key nutrient that controls phytoplankton growth in the Arabian Sea (Morrison et al. 1998); however, a model study showed that Si: N ratio is also important, particularly for the development of diatom bloom (Anju et al. 2020). CHEMTAX analysis revealed that diatoms contributed the most in the NFJ as reflected in marker pigments (Fuco, Chlc3, and DD),

and this was supported by microscopic analysis (Chowdhury et al. 2021). Diatoms have strategies to outcompete smaller phytoplankton in nutrient-rich waters (Falkowski and Oliver 2007; Cermeño et al. 2011) including fast nutrient uptake efficiency (Litchman et al. 2007), luxury uptake (Bandyopadhyay and Biswas, 2021), and storage (Thingstad et al. 2005). Thus, in this area, seasonal diatom blooms are common and respond much faster than any other phytoplankton group to nutrient upliftment by different physical forcing (upwelling, advection, convective mixing, etc.). In 2017, nitrogen depletion was more prominent in the NFJ as well as in the SFJ compared to 2018. Large diatom abundance was mostly restricted to the northernmost station (21° N) in 2017. A silicate depletion was detected in 2018 in the NFJ possibly due to the intake by large diatoms like *Rhizosolenia* (Chowdhury et al. 2021) and was also reported in earlier studies (Tarran et al. 1999).

While moving southward, downwelling-induced deeper MLDs were associated with low nutrient concentrations, and consistently, the contribution of diatoms to Chl_a decreased. The correlation between Chl_a and Fuco contents became weaker in this region suggesting a lower contribution of Fuco to total phytoplankton biomass in 2017, compared to 2018. The contribution of dinoflagellates derived from CHEMTAX showed enhanced abundance southward, especially in the upper 40 m in the AFJ and SFJ could be related to higher water temperature and low nutrient availability. Dinoflagellates can grow in diverse environmental conditions (Glibert et al. 2005) and are known as k-strategists which can thrive in areas with low N:P ratio, warm and moderate turbulent waters (Glibert et al. 2016). The dominance of small dinoflagellates such as *Gymnodinium* sp. *Gyrodinium* sp, and *Katodinium* sp. in the south of 15°N were also reported in the earlier studies (Garrison et al. 1998; Chowdhury et al. 2021). These mixotrophic dinoflagellates may also survive in this region as they can gain their nitrogen sources from heterotrophy and carbon sources by oxygenic photosynthesis at the same time (Mitra et al. 2016). Their ecological contribution has not been investigated in this region and should be addressed in future studies.

Usually, smaller phytoplankton can grow well in nitrogen-limited conditions due to their high surface area to volume ratio (Kiørboe 1993; Finkel et al. 2010; Marañón et al. 2012). Accordingly, the higher water temperature, and moderate to low nutrients in the AFJ and SFJ were occupied by nanophytoplankton and picophytoplankton during 2017 than in 2018. Among nanophytoplankton, the cooccurrence of prymnesiophytes (marker pigment 19'HF, 19'BF, and Chl_{c3}) indicated a higher abundance in 2017 in the AFJ and further extended toward the SFJ in 2018. Presumably, in the central Arabian Sea, the distribution of prymnesiophytes was primarily controlled by nutrient concentration rather than the water column stability. Prymnesiophytes are usually adaptable to wide environmental variability such as nutrient enrichment to nutrient-depletion, from hypo to hyper-saline, and from cold

to warm waters of the Arabian Sea (Barlow et al. 1999) as well as in the global ocean (Liu et al. 2009). Sub-surface waters in this region could be dominated by coccolithophores, the major prymnesiophytes from the Arabian Sea as evident from previous reports (Chowdhury et al. 2022). Coccolithophores are also well adapted to low light conditions (Carreto et al. 2008) and thus their dominance in the subsurface waters of the AFJ and SFJ can be justified. The presence of this group was also reported in the subsurface water of the Arabian Sea (Andrulleit et al. 2005) as well as in the Bay of Bengal (Bandyopadhyay et al. 2017) and was associated with the occurrence of nutricline. However, PAR data from this region would have strengthened the fact showing the impact of light on the distribution pattern of Coccolithophores. Studies from sediment trap (Andrulleit et al. 2000; Mergulhao et al. 2006) as well as water column (Andrulleit et al. 2005 and reference therein) documented coccolithophores in the coastal as well as the central Arabian Sea. Schiebel et al. (2004) noticed that coccolithophore abundance increased towards the open ocean with decreasing nutrients and increasing stratification.

The relative contribution of picophytoplankton was more confined towards the south in 2018 than in 2017 and could be related to stronger nitrogen limitation in 2017. Cyanobacteria (like *Synechococcus*) contributed the highest in the SFJ. Previous studies from this region recorded dominance of *Synechococcus* associated with low nutrients and high temperature (Burkill et al. 1993; Latasha and Bidigare 1998; Barlow et al. 1999; Brown et al. 2002). Moreover, in SFJ, the dominance of *Synechococcus* was restricted in the upper 20 m and could be due to the presence of primary pigments phycobiliproteins that absorb green light in the upper euphotic zone (Morel et al. 1993). Such patchy distribution could also be related to their strategy to escape grazing from protists (Brown et al. 2002). The presence of *prochlorophytes*, the other important picocyanobacteria containing DV-Chl *a+b* was detected from the surface to up to 60 m water depth. In *Prochlorococcus*, DV-Chl *a+b* and Mg 3,8 divinyl phaeoporphyrin *a₅* act as major light-harvesting pigments that can harvest blue light for photosynthesis at deeper depths (Ralf and Repeta 1992; Morel et al. 1993). Goericke et al. (2000) reported that *Prochlorococcus* was present in 80–120 m water depth from the OMZ of the Arabian Sea and contributed up to 97% to the pigment biomass. The absence of *prochlorophytes* in the NFJ suggested that the presence of cooler, nutrient-rich upwelled water was not preferred by this group. The contribution of *Prochlorococcus* was reduced significantly over a large area of the Arabian Sea during the summer monsoon-induced upwelling and increased during the intermonsoon season when nutrients were exhausted (Veldhuis and Kraay 1993; Veldhuis et al. 1997). Latasha and Bidigare (1998) proposed a mutual exclusion of diatoms and *Prochlorococcus* in the Arabian Sea and our observation is consistent with this hypothesis. Other than these groups, chlorophytes, and prasinophytes were the minor contributors to Chl *a* as well as to the total picophytoplankton group. The

former group was more confined to the AFJ and could be related to nutrients that were added by advection. The latter did not show any specific distribution pattern and contributed least to total phytoplankton biomass. Available literature from the Arabian Sea shows that they show similar distribution patterns as prymnesiophytes (Roy et al. 2015).

The observed spatiotemporal variability in phytoplankton size classes in the central Arabian Sea may considerably impact phytodetritus flux to the deep sea (Michaels and Silver 1988; Boyd and Newton 1999; Henson et al. 2019). The variability in phytoplankton communities driven by different physicochemical parameters may alter both the quality and quantity of organic matter export flux (Moriceau et al. 2018). A global database revealed that phytoplankton community composition could explain 68% of the variability in particle flux at 400 m (Guidi et al. 2009). The predominance of microphytoplankton dominated by diatoms in the NFJ during both years may induce higher export flux if they escape grazing. In the western and central Arabian Sea, copepods may remove nearly 50–100% of the diatom population by grazing (Landry et al. 1998; Smith et al. 1998; Gauns et al. 2005). However, large centric diatoms like *Coscinodiscus radiatus* (in 2017) and *Rhizosolenia* spp. (in 2018) (Chowdhury et al. 2021) could escape grazing (Jansen 2008; Löder et al. 2011) due to larger body size (Hansen et al. 1994) and can be exported to the lower mesopelagic. In another study, we analyzed the distribution and diversity of diatom frustules using 5 short sediment core top samples from the central Arabian Sea (Pandey et al. 2023). It was revealed that the NFJ and AFJ stations were dominated by large diatoms like *Coscinodiscus* and *Rhizosolenia*. Contrarily, the smaller and moderate-sized diatoms (*Thalassiosira*) were dominant at the surface sediments of SFJ. Likely, the larger diatom dominance induced by stronger upwelling may lead to the carbon flow to export flux rather than trophic transfer which can be better supported by small or moderate diatoms. On the other hand, nano and picoplankton may dominate the export flux in the south. Coccolithophore, a major part of the nanophytoplankton community from this region (Guptha et al. 1995; Andrulleit et al. 2004) could contribute significantly to export flux. Picophytoplankton can dominate the organic matter export flux in the open ocean of the equatorial Pacific Ocean as well as the Arabian Sea (Richardson and Jackson, 2007) and can take a longer trophic route via grazing (microzooplankton-mesozooplankton). However, they form an important part of the faecal matter production that contributes considerably to the export flux (Richardson 2018). Likewise, the higher picocyanobacteria dominance in the SFJ in 2017, might have a different impact on carbon export flux compared to 2018. Nevertheless, the efficiency of organic matter export from the upper mesopelagic to the abyssal plain can be significantly controlled by the presence and absence of oxygen-deficient waters within the mesopelagic (François et al. 2002; Keil et al. 2016).

Conclusion

Under the JGOFS program, phytoplankton community was monitored using both microscopy as well as pigments, particularly from the western and central Arabian Sea. In the context of Arabian Sea warming, it is important to understand how phytoplankton size class may shift (large to small and vice versa). A previous study described the microphytoplankton community composition in response to atmospheric forcings in the same study area during summer monsoons 2017-2018, however, it failed to document all size classes using microscopy. This is the first comprehensive study from the central Arabian Sea addressing phytoplankton size classes using chemotaxonomy (both CHEMTAX and manually derived) during consecutive summer monsoons after two decades of the JGOFS program. Both the methods revealed significant linearity indicating that the manual calculations can also be used in parallel with CHEMTAX software. We show here that spatiotemporal variability in phytoplankton size class distributions along the cruise track was modulated by upwelling/downwelling that was impacted by monsoon wind forcing. Microphytoplankton dominated by diatoms were found in the upwelling-impacted areas in the north. Our microscopic analysis also complemented this trend. The contribution of diatoms increased in 2018 induced by higher wind forcing and subsequent nutrient enrichment compared to 2017. This indicates that any future enhancement in monsoon wind forcing might increase diatom abundance impacting trophic transfer and organic matter export flux. Nanoplanktonic prymnesiophytes (e.g. coccolithophores) abundance increased with increasing depths and was associated with MLDs. Any possible change in MLDs due to warming/wind forcing may influence their distribution. Zeaxanthin-containing picocyanobacteria, which was mainly restricted to the south, was higher in 2017 relative to 2018 associated with warm, low-nutrient water. This signifies that in case of future warming and a weak monsoon, wind may lead to reduced advection and entrainment of nutrients promoting picocyanobacteria in this region. Such prevailing conditions may also support the growth of some heterotrophic/mixotrophic dinoflagellates. The north-south contrast in phytoplankton size classes might impact the efficiency of organic carbon transfer to higher trophic levels as well as export flux from the euphotic zone to the upper mesopelagic zone. However, the addition of flowcytometry data is recommended for future studies to add more specific information about the contribution of smaller phytoplankton.

Acknowledgments

This study was financially supported by the Council of Scientific and Industrial Research (CSIR) (MLP 1802). We are grateful to the Director National Institute of Oceanography-CSIR, for his support and encouragement. We express our sincere gratitude to Dr. Rajdeep Roy (Senior Scientist, Regional Remote Sensing Center, Kolkata, NRSC) for his guidance and help in using CHEMTAX software. We

are also thankful to the captain, scientists, technical staff, ship cell staff, crew members, deckhands, and the students onboard RV Sindhu Sadhna (SSD 040, SSD 55). We also acknowledge the help of Ms. Teja Naik for her help in HPLC analysis. The first author acknowledges CSIR for the CSIR-SRF fellowship (Grant no.: 31/26(0332)/2019-EMP-I). We are thankful to the anonymous reviewers for their valuable comments that substantially improved the manuscript. NIO contribution number is XXXX.

Authors contribution

HB contributed to the conception and design of the study. **MC** collected, analyzed the samples; organized the database, and performed the statistical analysis, and wrote the first draft of the manuscript. **HB**, **SS**, and **DS** participated in sample collection onboard and helped in accessory data generation. All authors contributed to the manuscript revision, read, and approved the submitted version.

Funding: The basic funding for this study was provided by the Council of Scientific and Industrial Research (CSIR). We acknowledge CSIR, the University Grant Commission (UGC), and the Department of Science and Technology (DST) for funding the first, third, and fourth authors.

Open Research Section: The data (Chowdhury et al. 2023) that support the findings of this study are available in Supporting Information and also openly accessible Mendeley Data, V2, <https://doi.org/10.17632/kjhfp2rsm6.2>

The surface (10 m) wind speed data was downloaded from the National Center for Environmental Prediction/National Centers for Atmospheric Research (NCEP/NCAR) reanalysis data (Kalnay et al. 1996) and can be obtained from <https://psl.noaa.gov/data/gridded/data.ncep.reanalysis.html>

Conflict of interest: The authors declare no competing interests.

Ethical Approval: Not Applicable

Consent to Participate: Not applicable

Consent to Publish Not applicable

References

- Aksnes, D. L., & Egge J. K. (1991) A theoretical model for nutrient uptake in phytoplankton. *Marine ecology progress series* Oldendorf 70: 65–72. <https://doi.org/10.3354/meps070065>
- Andrulleit, H., Rogalla, U., & Stäger, S. (2004) From living communities to fossil assemblages: origin and fate of coccolithophores in the northern Arabian Sea. *Micropaleontology*, 50(Suppl_1):5–21. https://doi.org/10.2113/50.Suppl_1.5

- Andrulleit, H., Rogalla, U., & Stäger, S. (2005) Living coccolithophores recorded during the onset of upwelling conditions off Oman in the western Arabian Sea. *Journal of Nannoplankton Research*, 27:1–14.
- Andrulleit, H. A., von Rad, U., Brans, A., & Ittekkot, V. (2000) Coccolithophore fluxes from sediment traps in the northeastern Arabian Sea off Pakistan. *Marine Micropaleontology* 38:285–308. [https://doi.org/10.1016/S0377-8398\(00\)00007-4](https://doi.org/10.1016/S0377-8398(00)00007-4)
- Anju, M., Sreesh, M. G., Valsala, V., Smitha, B. R., Hamza, F., Bharathi, G. et al. (2020) Understanding the role of nutrient limitation on plankton biomass over Arabian Sea via 1-D coupled biogeochemical model and bio-Argo observations. *Journal of Geophysical Research: Oceans* 125:e2019JC015502. <https://doi.org/10.1029/2019JC015502>
- Bandyopadhyay, D., Biswas, H., & Sarma, V. V. S. S. (2017) Impacts of SW Monsoon on Phytoplankton Community Structure Along the Western Coastal BOB: an HPLC Approach. *Estuary and Coast* 40:1066–1081. <https://doi.org/10.1007/s12237-016-0198-6>
- Bandyopadhyay, D., & Biswas, H. (2021). Impacts of variable nutrient stoichiometry (N, Si and P) on a coastal phytoplankton community from the SW Bay of Bengal, India. *European Journal of Phycology*, 56(3), 273-288. <https://doi.org/10.1080/09670262.2020.1834146>
- Banse, K., Naqvi, S. W. A., Narvekar, P. V., Postel, J. R., & Jayakumar D. A. (2014) Oxygen minimum zone of the open Arabian Sea: variability of oxygen and nitrite from daily to decadal timescales. *Biogeosciences* 11:2237–2261. <https://doi.org/10.5194/bg-11-2237-2014>
- Barlow, R. G., Mantoura, R. F. C., & Cummings, D. G. (1999) Monsoonal influence on the distribution of phytoplankton pigments in the Arabian Sea. *Deep Sea Research Part II: Topical Studies in Oceanography*, 46:677–699. [https://doi.org/10.1016/S0967-0645\(98\)00123-4](https://doi.org/10.1016/S0967-0645(98)00123-4)
- Bauer, S., Hitchcock, G. L., & Olson, D. B. (1991) Influence of monsoonally-forced Ekman dynamics upon surface layer depth and plankton biomass distribution in the Arabian Sea. *Deep Sea Research Part A. Oceanographic Research Papers* 38:531–553. [https://doi.org/10.1016/0198-0149\(91\)90062-K](https://doi.org/10.1016/0198-0149(91)90062-K)
- Boyd, P. W., & Newton, P. P. (1999) Does planktonic community structure determine downward particulate organic carbon flux in different oceanic provinces? *Deep Sea Research Part I: Oceanographic Research Papers* 46:63–91. [https://doi.org/10.1016/S0967-0637\(98\)00066-1](https://doi.org/10.1016/S0967-0637(98)00066-1)
- Boyd, P. W., & Trull, T. W. (2007) Understanding the export of biogenic particles in oceanic waters: Is there consensus? *Progress in Oceanography* 72:276–312. <https://doi.org/10.1016/j.pocean.2006.10.007>
- Brown, S. L., Landry, M. R., Christensen, S., Garrison, D., Gowing, M. M., Bidigare, R.R., & Campbell, L. (2002) Microbial community dynamics and taxon-specific phytoplankton production in the Arabian Sea during the 1995 monsoon seasons. *Deep Sea Research Part II: Topical Studies in Oceanography* 49:2345–2376. [https://doi.org/10.1016/S0967-0645\(02\)00040-1](https://doi.org/10.1016/S0967-0645(02)00040-1)
- Burkill, P.H., Leakey, R. J. G., Owens, N. J. P., & Mantoura, R. F. C. (1993) *Synechococcus* and its importance to the microbial food web of the northwestern Indian Ocean. *Deep-Sea Research II* 40:773–782. [https://doi.org/10.1016/0967-0645\(93\)90057-T](https://doi.org/10.1016/0967-0645(93)90057-T)

- Carreto, J. I., Montoya, N., Akselman, R., Carignan, M. O., Silva, R. I., & Colleoni, D. A. C. (2008) Algal pigment patterns and phytoplankton assemblages in different water masses of the Río de la Plata maritime front. *Continental Shelf Research* 28:1589–1606. <https://doi.org/10.1016/j.csr.2007.02.012>
- Cermeño, P., Lee, J. B., Wyman, K., Schofield, O., & Falkowski, P. G. (2011) Competitive dynamics in two species of marine phytoplankton under non-equilibrium conditions. *Marine ecology progress series* 429:19–28. <https://doi.org/10.3354/meps09088>
- Chisholm, S. W. (1992) Phytoplankton size. In: Falkowski PG, Woodhead AD (eds) *Primary Productivity and Biogeochemical Cycles in the Sea*, Plenum Press, New York, pp 213–237
- Chowdhury, M., Biswas, H., Mitra, A., Silori, S., Sharma, D., & Bandyopadhyay, D. et al. (2021) Southwest monsoon-driven changes in the phytoplankton community structure in the central Arabian Sea (2017–2018): After two decades of JGOFS. *Progress in Oceanography* 197:102654. <https://doi.org/10.1016/j.pocean.2021.102654>
- Chowdhury, M., Biswas, H., Sharma, D., Silori, S., & Winter, A. (2022). Distribution of extant coccolithophores from the northwest continental shelf of India during the summer monsoon. *Phycologia*, 61(3), 284-298. <https://doi.org/10.1080/00318884.2022.2037340>
- Chowdhury, M., Biswas, H, Silori, S., Sharma, D. (2023). “Interannual variability in phytoplankton size class distribution derived from pigment analysis in the central Arabian Sea (summer monsoon)”, Mendeley Data, V1 [Dataset]. <https://doi.org/10.17632/kjhfp2rsm6.2>
- Claustre, H. (1994) The trophic status of various oceanic provinces revealed by phytoplankton pigment signatures. *Limnology and Oceanography* 39:1206–1210. <https://doi.org/10.4319/lo.1994.39.5.1206>
- Edwards, M., & Richardson, A. J. (2004) Impact of climate change on marine pelagic phenology and trophic mismatch. *Nature* 430:881–884. <https://doi.org/10.1038/nature02808>
- Falkowski, P., & Knoll, A. H. (2011) *Evolution of primary producers in the sea*. Academic Press.
- Falkowski, P. G., & Oliver, M.J. (2007) Mix and match: how climate selects phytoplankton. *Nature reviews microbiology* 5(10):813–819. <https://doi.org/10.1038/nrmicro1751>
- Falkowski, P. G., & Raven, J. A. (2013) *Aquatic photosynthesis*. Princeton University Press.
- Field, C. B., Behrenfeld, M. J., Randerson, J. T., & Falkowski, P. (1998) Primary production of the biosphere: integrating terrestrial and oceanic components. *Science* 281:237–240. <https://doi.org/10.1126/science.281.5374.237>
- Findlater, J. (1969) A major low-level air current near the Indian Ocean during the northern summer. *Quarterly Journal of the Royal Meteorological Society* 95:362–380. <https://doi.org/10.1002/qj.49709540409>

- Finkel, Z. V., Beardall, J., Flynn, K. J., Quigg, A., Rees, T. A. V., & Raven, J. A. (2010) Phytoplankton in a changing world: cell size and elemental stoichiometry. *Journal of plankton research* 32:119–137. <https://doi.org/10.1093/plankt/fbp098>
- François, R., Honjo, S., Krishfield, R., & Manganini, S. (2002) Factors controlling the flux of organic carbon to the bathypelagic zone of the ocean. *Glob. Biogeochem. Cycles* 16:34–1. <https://doi.org/10.1029/2001GB001722>
- Garrison, D. L., Gowing, M. M., & Hughes, M. P. (1998) Nano- and microplankton in the northern Arabian Sea during the Southwest Monsoon, August-September, 1995: a US JGOFS study. *Deep-Sea Res. II Topical Studies in Oceanography* 45:2269–2300. [https://doi.org/10.1016/S0967-0645\(98\)00071-X](https://doi.org/10.1016/S0967-0645(98)00071-X)
- Gauns, M., Madhupratap, M., Ramaiah, N., Jyothibabu, R., Fernandes, V., Paul, J. T., & Kumar, S. P. (2005). Comparative accounts of biological productivity characteristics and estimates of carbon fluxes in the Arabian Sea and the Bay of Bengal. *Deep Sea Research Part II: Topical Studies in Oceanography*, 52(14-15), 2003-2017. <https://doi.org/10.1016/j.dsr2.2005.05.009>
- Glibert, P. M. (2016). Margalef revisited: a new phytoplankton mandala incorporating twelve dimensions, including nutritional physiology. *Harmful Algae*, 55, 25-30. <https://doi.org/10.1016/j.hal.2016.01.008>
- Glibert, P. M., Anderson, D. M., Gentien, P., Granéli, E., & Sellner, K. G. (2005). The global, complex phenomena of harmful algal blooms. <https://doi.org/10.5670/oceanog.2005.49>
- Goericke, R. (2002). Top-down control of phytoplankton biomass and community structure in the monsoonal Arabian Sea. *Limnology and Oceanography*, 47(5), 1307-1323. <https://doi.org/10.4319/lo.2002.47.5.1307>
- Goericke, R., Olson, R. J., & Shalapyonok, A. (2000). A novel niche for *Prochlorococcus* sp. in low-light suboxic environments in the Arabian Sea and the Eastern Tropical North Pacific. *Deep Sea Research Part I: Oceanographic Research Papers*, 47(7), 1183-1205. [https://doi.org/10.1016/S0967-0637\(99\)00108-9](https://doi.org/10.1016/S0967-0637(99)00108-9)
- Goes, J.I., & Gomes, H. D. R. (2016) An Ecosystem in Transition: The Emergence of Mixotrophy in the Arabian Sea. in *Aquatic Microbial Ecology and Biogeochemistry: A Dual Perspective* eds P. Glibert, T. Kana (Springer, Cham: Springer International Publishing) https://doi.org/10.1007/978-3-319-30259-1_13
- Grasshoff, K., Kremling, K., & Ehrhardt, M. (2009) *Methods of seawater analysis*. New Jersey, John Wiley & Sons.
- Guidi, L., Stemann, L., Jackson, G. A., Ibanez, F., Claustre, H., Legendre, L. et al. (2009) Effects of phytoplankton community on production, size, and export of large aggregates: A world-ocean analysis. *Limnology and Oceanography* 54:1951–1963. <https://doi.org/10.4319/lo.2009.54.6.1951>
- Guptha, M. V. S., Mohan, R., & Muralinath, A. S. (1995). Living coccolithophorids from the Arabian Sea. *Oceanographic Literature Review*, 11(42), 992.
- Haake, B., Ittekkot, V., Rixen, T., Ramaswamy, V., Nair, R. R., & Curry, W. B. (1993). Seasonality and interannual variability of particle fluxes to the deep Arabian Sea. *Deep Sea Research Part I:*

Oceanographic Research Papers, 40(7), 1323-1344.[https://doi.org/10.1016/0967-0637\(93\)90114-I](https://doi.org/10.1016/0967-0637(93)90114-I)

- Hammer, Ø., Harper, D. A. T., & Ryan, P. D. (2001) PAST: Paleontological Statistics Software Package for Education and Data Analysis (Version 4) [Software]. Palaeontologia Electronica. http://palaeo-electronica.org/2001_1/past/issue1_01.htm.
- Hansen, B., Bjornsen, P. K., & Hansen, P. J. (1994). The size ratio between planktonic predators and their prey. *Limnology and Oceanography*, 39(2), 395-403.<https://doi.org/10.4319/lo.1994.39.2.0395>
- Henson, S., Le Moigne, F., & Giering, S. (2019). Drivers of carbon export efficiency in the global ocean. *Global biogeochemical cycles*, 33(7), 891-903.<https://doi.org/10.1029/2018GB006158>
- Jansen, S. (2008). Copepods grazing on *Coscinodiscus wailesii*: a question of size?. *Helgoland Marine Research*, 62(3), 251-255.<https://doi.org/10.1007/s10152-008-0113-z>
- Jennings, S., & Warr, K. J., Mackinson S (2002) Use of size-based production and stable isotope analyses to predict trophic transfer efficiencies and predator-prey body mass ratios in food webs. *Marine Ecology Progress Series* 240:11–20. <https://doi.org/10.3354/meps240011>
- Kalnay, E., Kanamitsu, M., Kistler, R., Collins, W., Deaven, D., Gandin, L., Zhu, Y. (1996), The NCEP/NCAR40-yearreanalysisproject. *Bulletin of American Meteorological Society*, 77, 437–471 [Dataset]. [https://doi.org/10.1175/1520-0477\(1996\)077%3C0437:TNYRP%3E2.0.CO;2](https://doi.org/10.1175/1520-0477(1996)077%3C0437:TNYRP%3E2.0.CO;2)
- Kawamiya, M. (2001) Mechanism of offshore nutrient supply in the Western Arabian Sea. *Journal of Marine Research* 59:675–696. <https://doi.org/10.1357/002224001762674890>
- Keil, R. G., Neibauer, J. A., Biladeau, C., van der Elst, K., & Devol, A. H. (2016). A multiproxy approach to understanding the "enhanced" flux of organic matter through the oxygen-deficient waters of the Arabian Sea. *Biogeosciences*, 13(7), 2077-2092.<https://doi.org/10.5194/bg-13-2077-2016>
- Kjørboe, T. (1993) Turbulence, phytoplankton cell size, and the structure of pelagic food webs. *Advances in marine biology* 29:1–72.
- Klausmeier, C. A., Litchman, E., Daufresne, T., & Levin, S. A. (2008). Phytoplankton stoichiometry. *Ecological Research*, 23(3), 479-485.<https://doi.org/10.1007/s11284-008-0470-8>
- Knap, A. H., Michaels, A., Close, A. R., Ducklow, H., & Dickson, A. G. (1996). Protocols for the joint global ocean flux study (JGOFS) core measurements. JGOFS, Reprint of the IOC Manuals and Guides No. 29, UNESCO 1994, 19.
- Landry, M. R., Brown, S. L., Campbell, L., Constantinou, J., & Liu, H. (1998). Spatial patterns in phytoplankton growth and microzooplankton grazing in the Arabian Sea during monsoon forcing. *Deep Sea Research Part II: Topical Studies in Oceanography*, 45(10-11), 2353-2368.[https://doi.org/10.1016/S0967-0645\(98\)00074-5](https://doi.org/10.1016/S0967-0645(98)00074-5)
- Latasa, M., & Bidigare, R. R. (1998) A comparison of phytoplankton populations of the Arabian Sea during the Spring Intermonsoon and Southwest Monsoon of 1995 as described by HPLC-analyzed pigments. *Deep Sea Research Part II: Topical Studies in Oceanography* 45:2133–2170. [https://doi.org/10.1016/S0967-0645\(98\)00066-6](https://doi.org/10.1016/S0967-0645(98)00066-6)

- Lee, C. M., Jones, B. H., Brink, K. H., & Fischer, A. S. (2000). The upper-ocean response to monsoonal forcing in the Arabian Sea: seasonal and spatial variability. *Deep Sea Research Part II: Topical Studies in Oceanography*, 47(7-8), 1177-1226. [https://doi.org/10.1016/S0967-0645\(99\)00141-1](https://doi.org/10.1016/S0967-0645(99)00141-1)
- Legendre, L., & Lefevre, J. (1989) "Hydrodynamical singularities as controls of recycled versus export production in oceans," in *Productivity of the Ocean: Present and Past*, eds W. H. Berger, V. S. Smetacek, and G. Wefer (Chichester: Wiley), 49–63.
- Leps, J. & Šmilauer, P.,(2003). *Multivariate analysis of ecological data using CANOCO*. Cambridge University Press, Cambridge, UK. 282 pp.
- Levitus, S. (1982) *Climatological atlas of the world ocean (Vol. 13)*. US Department of Commerce, National Oceanic and Atmospheric Administration.
- Lévy, M., Shankar, D., André, J. M., Shenoi, S. S. C., Durand, F., & de Boyer Montégut, C. (2007). Basin-wide seasonal evolution of the Indian Ocean's phytoplankton blooms. *Journal of Geophysical Research: Oceans*, 112(C12).<https://doi.org/10.1029/2007JC004090>
- Liao, X., Zhan, H., & Du, Y. (2016). Potential new production in two upwelling regions of the western Arabian Sea: Estimation and comparison. *Journal of Geophysical Research: Oceans*, 121(7), 4487-4502. <https://doi.org/10.1002/2016JC011707>
- Lichtman, E., & Klausmeier, C. A. (2008) Trait based community ecology of phytoplankton. *Annu. Rev. Ecol. Evol. Syst.* 39:615–639. <https://doi.org/10.1146/annurev.ecolsys.39.110707.173549>
- Litchman, E., Klausmeier, C. A., Schofield, O. M., & Falkowski, P. G. (2007). The role of functional traits and trade-offs in structuring phytoplankton communities: scaling from cellular to ecosystem level. *Ecology letters*, 10(12), 1170-1181.<https://doi.org/10.1111/j.1461-0248.2007.01117.x>
- Liu, H., Probert, I., Uitz, J., Claustre, H., Aris-Brosou, S., Frada, M., et al. (2009). Extreme diversity in noncalcifying haptophytes explains a major pigment paradox in open oceans. *Proceedings of the national academy of sciences*, 106(31), 12803-12808..<https://doi.org/10.1073/pnas.0905841106>
- Löder, M. G., Meunier, C., Wiltshire, K. H., Boersma, M., & Aberle, N. (2011). The role of ciliates, heterotrophic dinoflagellates and copepods in structuring spring plankton communities at Helgoland Roads, North Sea. *Marine biology*, 158(7), 1551-1580.<https://doi.org/10.1007/s00227-011-1670-2>
- Lotliker, A. A., Baliarsingh, S. K., Trainer, V. L., Wells, M. L., Wilson, C., Bhaskar, T. U., et al. (2018). Characterization of oceanic Noctiluca blooms not associated with hypoxia in the Northeastern Arabian Sea. *Harmful Algae*, 74, 46-57.<https://doi.org/10.1016/j.hal.2018.03.008>
- Mackey, M.D., Mackey, D.J., Higgins, H.W. & Wright, S.W., (1996). CHEMTAX-a program for estimating class abundances from chemical markers: application to HPLC measurements of phytoplankton. *Marine Ecology Progress Series*, 144, 265-283. <https://doi.org/10.3354/meps144265>
- Marañón, E., Cermeno, P., Latasa, M., & Tadonléké, R. D. (2012). Temperature, resources, and phytoplankton size structure in the ocean. *Limnology and Oceanography*, 57(5), 1266-1278.<https://doi.org/10.4319/lo.2012.57.5.1266>

- Margalef, R. (1978). Life-forms of phytoplankton as survival alternatives in an unstable environment. *Oceanol. Acta* 1: 493–509.
- Martin, J. H., Gordon, R. M., & Fitzwater, S. E. (1990). Iron in Antarctic waters. *Nature*, 345(6271), 156-158. <https://doi.org/10.1038/345156a0>
- Mergulhao, L. P., Mohan, R., Murty, V. S. N., Guptha, M. V. S., & Sinha, D. K. (2006). Coccolithophores from the central Arabian Sea: Sediment trap results. *Journal of earth system science*, 115(4), 415-428. <https://doi.org/10.1007/BF02702870>
- Michaels, A. F., & Silver, M. W. (1988). Primary production, sinking fluxes and the microbial food web. *Deep Sea Research Part A. Oceanographic Research Papers*, 35(4), 473-490. [https://doi.org/10.1016/0198-0149\(88\)90126-4](https://doi.org/10.1016/0198-0149(88)90126-4)
- Mitra, A., Flynn, K.J., Tillmann, U., Raven, J.A., Caron, D., Stoecker, D.K., Not, F., Hansen, P.J., Hallegraeff, G., Sanders, R. and Wilken, S., (2016). Defining planktonic protist functional groups on mechanisms for energy and nutrient acquisition: incorporation of diverse mixotrophic strategies. *Protist*, 167(2), 106-120. <https://doi.org/10.1016/j.protis.2016.01.003>
- Morel, A., Ahn, Y. H., Partensky, F., Vaultot, D., & Claustre, H. (1993). Prochlorococcus and Synechococcus: a comparative study of their optical properties in relation to their size and pigmentation. *Journal of Marine Research*, 51(3), 617-649. <https://doi.org/10.1357/0022240933223963>
- Moriceau, B., Iversen, M. H., Gallinari, M., Evertsen, A. J. O., Le Goff, M., Beker, B., et al. (2018). Copepods boost the production but reduce the carbon export efficiency by diatoms. *Frontiers in Marine Science*, 5, 82. <https://doi.org/10.3389/fmars.2021.773481>
- Morrison, J. M., Codispoti, L. A., Gaurin, S., Jones, B., Manghnani, V., & Zheng, Z. (1998). Seasonal variation of hydrographic and nutrient fields during the US JGOFS Arabian Sea Process Study. *Deep Sea Research Part II: Topical Studies in Oceanography*, 45(10-11), 2053-2101. [https://doi.org/10.1016/S0967-0645\(98\)00063-0](https://doi.org/10.1016/S0967-0645(98)00063-0)
- Pandey, M., Biswas, H., & Chowdhury, M. (2023). Interlinking diatom frustule diversity from the abyss of the central Arabian Sea to surface processes: physical forcing and oxygen minimum zone. *Environmental Monitoring and Assessment*, 195(1), 1-19. <https://doi.org/10.1007/s10661-022-10749-7>
- PrasannaKumar, S, Madhupratap, M., Kumar, M. D., Muraleedharan, P. M., De Souza, S. N., Gauns, M., & Sarma, V. V. S. S. (2001). High biological productivity in the central Arabian Sea during the summer monsoon driven by Ekman pumping and lateral advection. *Current Science*, 1633-1638.
- PrasannaKumar, S., Roshin, R. P., Narvekar, J., Kumar, P. D., & Vivekanandan, E. (2009). Response of the Arabian Sea to global warming and associated regional climate shift. *Marine Environmental Research*, 68(5), 217-222. <https://doi.org/10.1016/j.marenvres.2009.06.010>
- Ralf, G., & Repeta, D. J. (1992). The pigments of *Prochlorococcus marinus*: The presence of divinylchlorophyll a and b in a marine procaryote. *Limnology and Oceanography*, 37(2), 425-433. <https://doi.org/10.4319/lo.1992.37.2.0425>

- Ramage, C. S. (1987) "Monsoon Climates", in *The Encyclopedia of Climatology*, eds J. E. Oliver and R. W. Fairbridge (Van Nostrand Reinhold Company, New York).
- Richardson, T. L. (2019) Mechanisms and pathways of small-phytoplankton export from the surface ocean. *Annual review of marine science* 11:57–74. <https://doi.org/10.1146/annurev-marine-121916-063627>
- Richardson, T.L., & Jackson G. A., (2007) Small phytoplankton and carbon export from the surface ocean. *Science* 315: 838–840. <https://doi.org/10.1126/science.1133471>
- Rixen, T., Haake, B., Ittekkot, V., Guptha, M. V. S., Nair, R. R., & Schlüssel, P. (1996). Coupling between SW monsoon-related surface and deep ocean processes as discerned from continuous particle flux measurements and correlated satellite data. *Journal of Geophysical Research: Oceans*, 101(C12), 28569-28582. <https://doi.org/10.1029/96JC02420>
- Rixen, T., Cowie, G., Gaye, B., Goes, J., do Rosário Gomes, H., Hood, R. R., ... & Singh, A. (2020). Reviews and syntheses: Present, past, and future of the oxygen minimum zone in the northern Indian Ocean. *Biogeosciences*, 17(23), 6051-6080. <https://doi.org/10.5194/bg-17-6051-2020>
- Rixen, T., Gaye, B., & Emeis, K. C. (2019). The monsoon, carbon fluxes, and the organic carbon pump in the northern Indian Ocean. *Progress in oceanography*, 175, 24-39. <https://doi.org/10.1016/j.pocean.2019.03.001>
- Rousseaux, C. S., & Gregg, W. W. (2015). Recent decadal trends in global phytoplankton composition. *Global Biogeochemical Cycles*, 29(10), 1674-1688. <https://doi.org/10.1002/2015GB005139>
- Roy, R., Chitari, R., Kulkarni, V., Krishna, M.S., Sarma, V.V.S.S. & Anil, A.C. (2015). CHEMTAX-derived phytoplankton community structure associated with temperature fronts in the northeastern Arabian Sea. *Journal of Marine Systems*, 144, 81-91. <https://doi.org/10.1016/j.jmarsys.2014.11.009>
- Roxy, M. K. (2017). Land warming revives monsoon. *Nature Climate Change*, 7(8), 549-550. <https://doi.org/10.1175/JCLI-D-14-00471.1>
- Sawant, S., Madhupratap, M. (1996) Seasonality and composition of phytoplankton in the Arabian Sea. *Current Science* 71:869–873
- Schiebel, R., Zeltner, A., Treppke, U. F., Waniek, J. J., Bollmann, J., Rixen, T., & Hemleben, C. (2004). Distribution of diatoms, coccolithophores and planktic foraminifers along a trophic gradient during SW monsoon in the Arabian Sea. *Marine Micropaleontology*, 51(3-4), 345-371. <https://doi.org/10.1016/j.marmicro.2004.02.001>
- Sharma, S., Ha, K. J., Yamaguchi, R., Rodgers, K. B., Timmermann, A., & Chung, E. S. (2023). Future Indian Ocean warming patterns. *Nature Communications*, 14(1), 1789. <https://doi.org/10.1038/s41467-023-37435-7>
- Sieburth, J. M., Smetacek, V., & Lenz, J. (1978). Pelagic ecosystem structure: Heterotrophic compartments of the plankton and their relationship to plankton size fractions 1. *Limnology and Oceanography*, 23(6), 1256-1263. <https://doi.org/10.4319/lo.1978.23.6.1256>
- Silori, S., Sharma, D., Chowdhury, M., Biswas, H., Cardinal, D., & Mandeng-Yogo, M. (2021). Particulate organic matter dynamics and its isotopic signatures ($\delta^{13}\text{C}_{\text{POC}}$ and $\delta^{15}\text{N}_{\text{PN}}$) in relation to

- physical forcing in the central Arabian Sea during SW monsoon (2017–2018). *Science of the Total Environment*, 785, 147326.<https://doi.org/10.1016/j.scitotenv.2021.147326>
- Smith, S., Roman, M., Prusova, I., Wishner, K., Gowing, M., Codispoti, L. A., et al. (1998). Seasonal response of zooplankton to monsoonal reversals in the Arabian Sea. *Deep Sea Research Part II: Topical Studies in Oceanography*, 45(10-11), 2369-2403.[https://doi.org/10.1016/S0967-0645\(98\)00075-7](https://doi.org/10.1016/S0967-0645(98)00075-7)
- Tarran, G. A., Burkill, P. H., Edwards, E. S., & Woodward, E. M. S. (1999). Phytoplankton community structure in the Arabian Sea during and after the SW monsoon, 1994. *Deep Sea Research Part II: Topical Studies in Oceanography*, 46(3-4), 655-676.[https://doi.org/10.1016/S0967-0645\(98\)00122-2](https://doi.org/10.1016/S0967-0645(98)00122-2)
- Ter Braak, C. J. F., Šmilauer, P. (2002) *CANOCO Reference Manual and User's Guide to Canoco for Windows: Software for Canonical Community Ordination (Version 4.53)* [Software]. Microcomputer power, Ithaca, NY.
- Thingstad, T. F., Øvreås, L., Egge, J. K., Løvdal, T., & Haldal, M. (2005). Use of non-limiting substrates to increase size; a generic strategy to simultaneously optimize uptake and minimize predation in pelagic osmotrophs?. *Ecology Letters*, 8(7), 675-682.[doi:10.1111/j.1461-0248.2005.00768.x](https://doi.org/10.1111/j.1461-0248.2005.00768.x)
- Twining, B. S., & Baines, S. B. (2013) The trace metal composition of marine phytoplankton. *Annual review of marine science* 5:191–215. <https://doi.org/10.1146/annurev-marine-121211-172322>
- Uitz, J., Claustre, H., Morel, A., & Hooker, S. B. (2006). Vertical distribution of phytoplankton communities in open ocean: An assessment based on surface chlorophyll. *Journal of Geophysical Research: Oceans*, 111(C8).<https://doi.org/10.1029/2005JC003207>
- Utermöhl, H. (1958) Methods of collecting plankton for various purposes are discussed. *International Association for Theoretical and Applied Limnology: Mitteilungen* 9:1–38. <https://doi.org/10.1080/05384680.1958.11904091>
- Van Heukelem, L., & Thomas, C.S. (2001). Computer-assisted high-performance liquid chromatography method development with applications to the isolation and analysis of phytoplankton pigments. *J. Chromatogr. A* 910:31–49. [https://doi.org/10.1016/S0378-4347\(00\)00603-4](https://doi.org/10.1016/S0378-4347(00)00603-4)
- Veldhuis, M. J., & Kraay, G. W. (1993). Cell abundance and fluorescence of picoplankton in relation to growth irradiance and nitrogen availability in the Red Sea. *Netherlands Journal of Sea Research*, 31(2), 135-145.[https://doi.org/10.1016/0077-7579\(93\)90003-B](https://doi.org/10.1016/0077-7579(93)90003-B)
- Veldhuis, M. J., Kraay, G. W., Van Bleijswijk, J. D., & Baars, M. A. (1997). Seasonal and spatial variability in phytoplankton biomass, productivity and growth in the northwestern Indian Ocean: the southwest and northeast monsoon, 1992–1993. *Deep Sea Research Part I: Oceanographic Research Papers*, 44(3), 425-449.[https://doi.org/10.1016/S0967-0637\(96\)00116-1](https://doi.org/10.1016/S0967-0637(96)00116-1)
- Vidussi, F., Claustre, H., Manca, B. B., Luchetta, A., & Marty, J. C. (2001). Phytoplankton pigment distribution in relation to upper thermocline circulation in the eastern Mediterranean Sea during winter. *Journal of Geophysical Research: Oceans*, 106(C9), 19939-19956.<https://doi.org/10.1029/1999JC000308>

- Wright, S. W., & Jeffrey, S. W. (2006). Pigment markers for phytoplankton production. *Marine Organic Matter* 2:71–104. https://doi.org/10.1007/698_2_003
- Wright, S.W., Thomas, D.P., Marchant, H.J., Higgins, H.W., Mackey, M.D. & Mackey, D.J. (1996). Analysis of phytoplankton of the Australian sector of the Southern Ocean: comparisons of microscopy and size frequency data with interpretations of pigment HPLC data using the ‘CHEMTAX’ matrix factorisation program. *Marine Ecology Progress Series*, 144, 285-298. <https://doi.org/10.3354/meps144285>
- Wright, S.W., Ishikawa, A., Marchant, H.J., Davidson, A.T., van den Enden, R.L. & Nash, G.V., (2009). Composition and significance of picophytoplankton in Antarctic waters. *Polar Biology*, 32, 797-808. <https://doi.org/10.1007/s00300-009-0582-9>
- Wright, S.W., van den Enden, R.L., Pearce, I., Davidson, A.T., Scott, F.J. & Westwood, K.J., (2010). Phytoplankton community structure and stocks in the Southern Ocean (30–80 E) determined by CHEMTAX analysis of HPLC pigment signatures. *Deep Sea Research Part II: Topical Studies in Oceanography*, 57(9-10), 758-778. <https://doi.org/10.1016/j.dsr2.2009.06.015>
- Xiang, C., Tan, Y., Zhang, H., Liu, J., Ke, Z., & Li, G. (2019). Xiang, C., Tan, Y., Zhang, H., Liu, J., Ke, Z., & Li, G. (2019). The key to dinoflagellate (*Noctiluca scintillans*) blooming and outcompeting diatoms in winter off Pakistan, northern Arabian Sea. *Science of The Total Environment*, 694, 133396. <https://doi.org/10.1016/j.scitotenv.2019.07.202>
- Young, D. K., & Kindle, J. C. (1994). Physical processes affecting availability of dissolved silicate for diatom production in the Arabian Sea. *Journal of Geophysical Research: Oceans*, 99(C11), 22619-22632. <https://doi.org/10.1029/94jc01449>
- Zhang, Z., Ma, W., & Chai, F. (2022). Role of ocean circulation and settling of particulate organic matter in the decoupling between the oxygen minimum zone and the phytoplankton productive zone in the Arabian Sea: A modeling study. *Frontiers in Marine Science*, 9, 927921. <https://doi.org/10.3389/fmars.2022.927921>

Figure legends

Figure 1 Monthly-averaged reanalysis wind data with a resolution of $1^\circ \times 1^\circ$ were obtained from the National Centre for Environmental Prediction (NCEP), Maryland, USA, an open-access library for the entire study region (Kalnay et al. 1996) (<http://www.cdc.noaa.gov/cdc/data.ncep.reanalysis.html>) during (A) 2017 and (B) 2018. Station locations are shown in white circles. Latitudinal distribution of Mixed Layer Depths (MLD) along the central Arabian Sea during the summer monsoon 2017 and 2018 in the central Arabian Sea (C).

Figure 2 Vertical profiles of water temperature (A, B) (white contour lines represent D_{24} isotherm), salinity (C, D), and dissolved oxygen (DO) (E, F) (white contour lines represent 2.5 ml l^{-1} isoline) during summer monsoon of 2017 (left panel) and 2018 (right panel) in the central Arabian Sea.

Figure 3 Cross-sectional profiles of the concentrations of nitrate+nitrite (A, B) (white contour lines represent $5.0 \mu\text{M l}^{-1}$ isoline), DIP (C, D) (white contour lines represent $1.0 \mu\text{M l}^{-1}$ isoline), DSi (E, F) (white contour lines represent $2.5 \mu\text{M l}^{-1}$ isoline), the ratios of Si: N (DSi:nitrate+nitrite) (G, H) and N:P (nitrate+nitrite:DIP) (I, J) during the summer monsoon 2017 (left panel) and 2018 (right panel) in the central Arabian Sea.

Figure 4 Latitudinal distributions of the concentrations of TChla (A, B), DV-Chla (C, D), fucoxanthin (E, F), and peridinin (G, H) during the summer monsoon 2017 (left panel) and 2018 (right panel) in the central Arabian Sea.

Figure 5 Latitudinal distributions of the concentrations of 19'HF (A, B), 19'BF (C, D), zeaxanthin (E, F), and chlorophyll *b* (G, H) during the summer monsoon 2017 and 2018 in the central Arabian Sea.

Figure 6 Cross-sectional profile of the relative percentage contributions of the major phytoplankton groups Diatoms (A, B), Dinoflagellates (C, D), Prymnesiopytes (E, F), Cyanobacteria (G, H), and Prochlorophytes (I, J) to total chlorophyll *a* estimated by the CHEMTAX program using marker pigments during the summer monsoon 2017 (left panel) and 2018 (right panel) in the central Arabian Sea.

Figure 7 Correlations between the set of values of different size classes of phytoplankton manually derived and CHEMTAX analysis highlighting the significant linearity ($p < 0.0001$, $n = 140$).

Figure 8 Cross-sectional profiles of different size classes of phytoplankton showing microphytoplankton (A, B), nanophytoplankton (C, D), and picophytoplankton (E, F) during the summer monsoon 2017 and 2018 in the central Arabian Sea.

Figure 9 Correlation matrix between physicochemical parameters and phytoplankton major groups as well as size classes of (A) 2017 and (B) 2018. Only significant correlations ($p < 0.05$) are presented here and the correlation values ranged between -1 (dark red) to +1 (dark blue). RDA biplot showing the interrelationship between physicochemical parameters (red arrow) and phytoplankton size classes and major groups (blue arrow) during (C) 2017 and (D) 2018. Phytoplankton cell abundance (cell abund.) of microscopic analysis from Chowdhury et al. (2021) has been considered to validate the microphytoplankton contribution. Abbreviations: Temp: temperature; DO: dissolved oxygen; Sal: salinity; MLD: mixed layer depth; $\text{NO}_2 + \text{NO}_3$: nitrate+nitrite; DSi: dissolved inorganic silicate; DIP: dissolved inorganic phosphate; Chla: Chlorophyll *a*; Micro: microphytoplankton; Nano: nanophytoplankton.

Table 1: Average value of the physicochemical parameters, the marker pigment concentrations (\pm SD), and single-factor ANOVA (at 95% confidence level) for 2017 and 2018. The significant probability (p) values are marked in **bold**.

Parameter	2017	2018	Level of significance
Wind speed	8.70 \pm 0.37	10.24 \pm 0.75	$p < 0.001$
MLD	77 \pm 23	97 \pm 34	$p < 0.13$
Salinity	36.40 \pm 0.09	36.43 \pm 0.11	$p < 0.65$
Temperature ($^{\circ}$ C)	27.04 \pm 0.70	26.21 \pm 0.55	$p < 0.001$
Dissolve oxygen (ml L $^{-1}$)	4.31 \pm 0.48	4.04 \pm 0.40	$p < 0.001$
DIN (μ mol L $^{-1}$)	2.0 \pm 2.96	4.50 \pm 2.69	$p < 0.001$
DSi (μ mol L $^{-1}$)	1.53 \pm 0.78	2.17 \pm 1.36	$p < 0.001$
DIP (μ mol L $^{-1}$)	0.51 \pm 0.30	0.90 \pm 0.36	$p < 0.001$
N:P	3.66 \pm 3.36	5.18 \pm 2.31	$p < 0.01$
Si:N	4.19 \pm 10.77	0.54 \pm 0.36	$p < 0.01$
Tchl a	0.32 \pm 0.16	0.32 \pm 0.13	$p < 0.93$
Fuco (μ g L $^{-1}$)	0.029 \pm 0.038	0.043 \pm 0.044	$p < 0.05$
Perid (μ g L $^{-1}$)	0.006 \pm 0.005	0.005 \pm 0.002	$p < 0.05$
19'HF (μ g L $^{-1}$)	0.035 \pm 0.019	0.034 \pm 0.013	$p < 0.76$
Zea (μ g L $^{-1}$)	0.046 \pm 0.045	0.030 \pm 0.023	$p < 0.01$
DV-Chl a (μ g L $^{-1}$)	0.021 \pm 0.012	0.021 \pm 0.008	$p < 0.85$

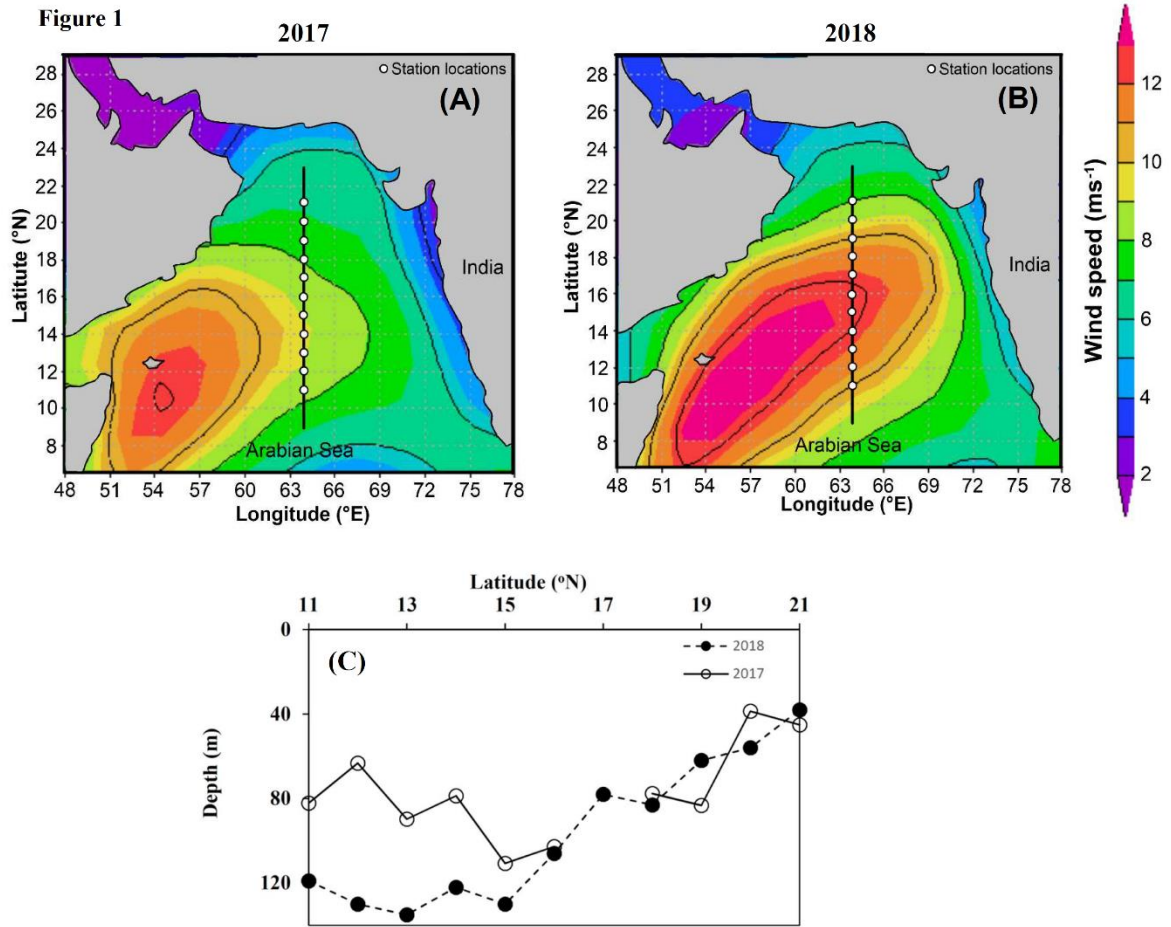


Figure 1 Monthly-averaged reanalysis wind data with a resolution of $1^\circ \times 1^\circ$ were obtained from the National Centre for Environmental Prediction (NCEP), Maryland, USA, an open-access library for the entire study region (Kalnay et al. 1996) (<http://www.cdc.noaa.gov/cdc/data.ncep.reanalysis.html>) during (A) 2017 and (B) 2018. Station locations are shown in white circles. Latitudinal distribution of Mixed Layer Depths (MLD) along the central Arabian Sea during the summer monsoon 2017 and 2018 in the central Arabian Sea (C).

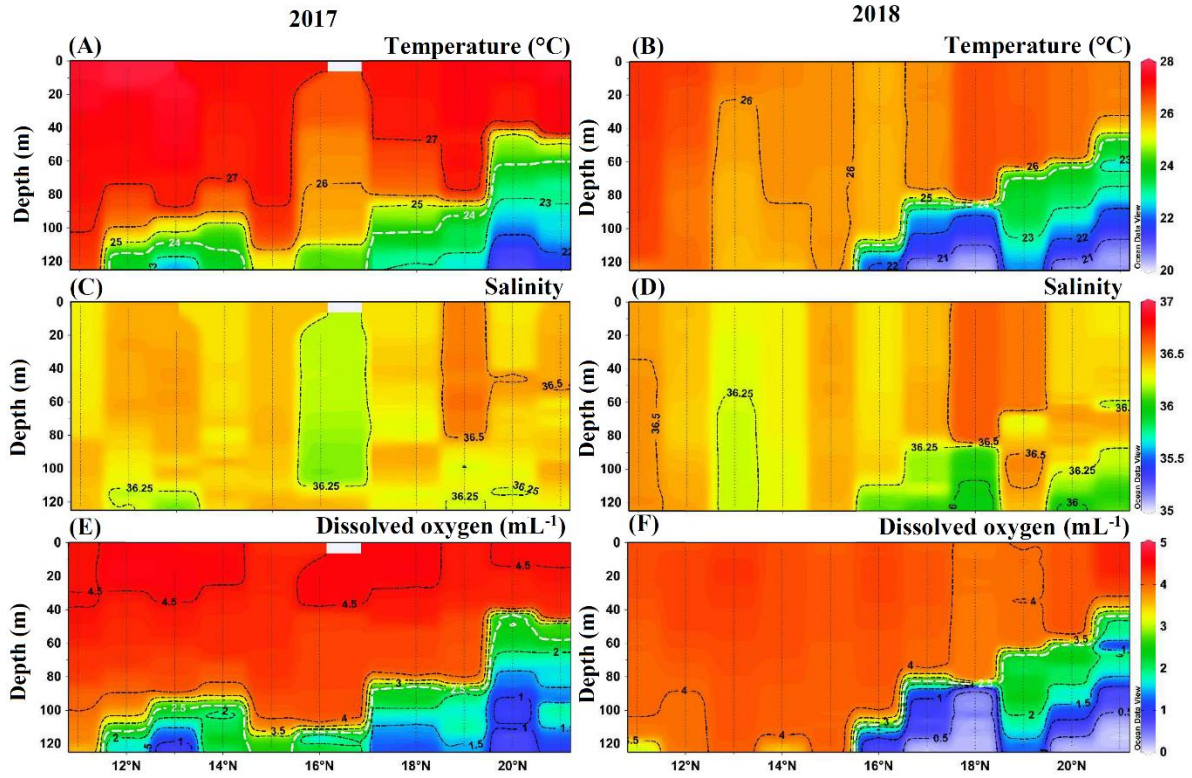


Figure 2 Vertical profiles of water temperature (A, B) (white contour lines represent D_{24} isotherm), salinity (C, D), and dissolved oxygen (DO) (E, F) (white contour lines represent 2.5 ml l^{-1} isoline) during summer monsoon of 2017 (left panel) and 2018 (right panel) in the central Arabian Sea.

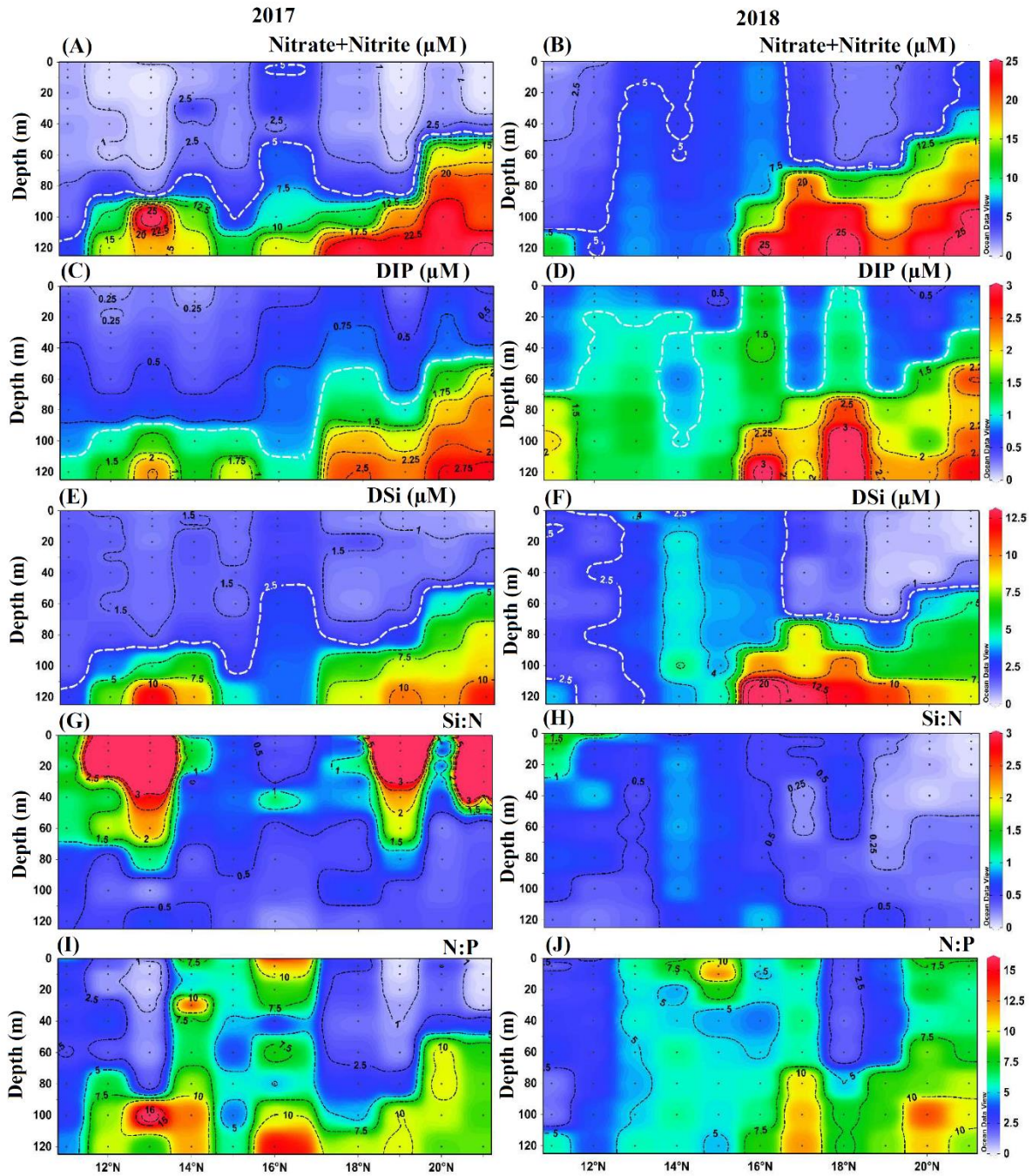


Figure 3 Cross-sectional profiles of the concentrations of nitrate+nitrite (**A, B**) (white contour lines represent $5.0 \mu\text{M l}^{-1}$ isoline), DIP (**C, D**) (white contour lines represent $1.0 \mu\text{M l}^{-1}$ isoline), DSi (**E, F**) (white contour lines represent $2.5 \mu\text{M l}^{-1}$ isoline), the ratios of Si: N (DSI:nitrate+nitrite) (**G, H**) and N:P (nitrate+nitrite:DIP) (**I, J**) during the summer monsoon 2017 (left panel) and 2018 (right panel) in the central Arabian Sea.

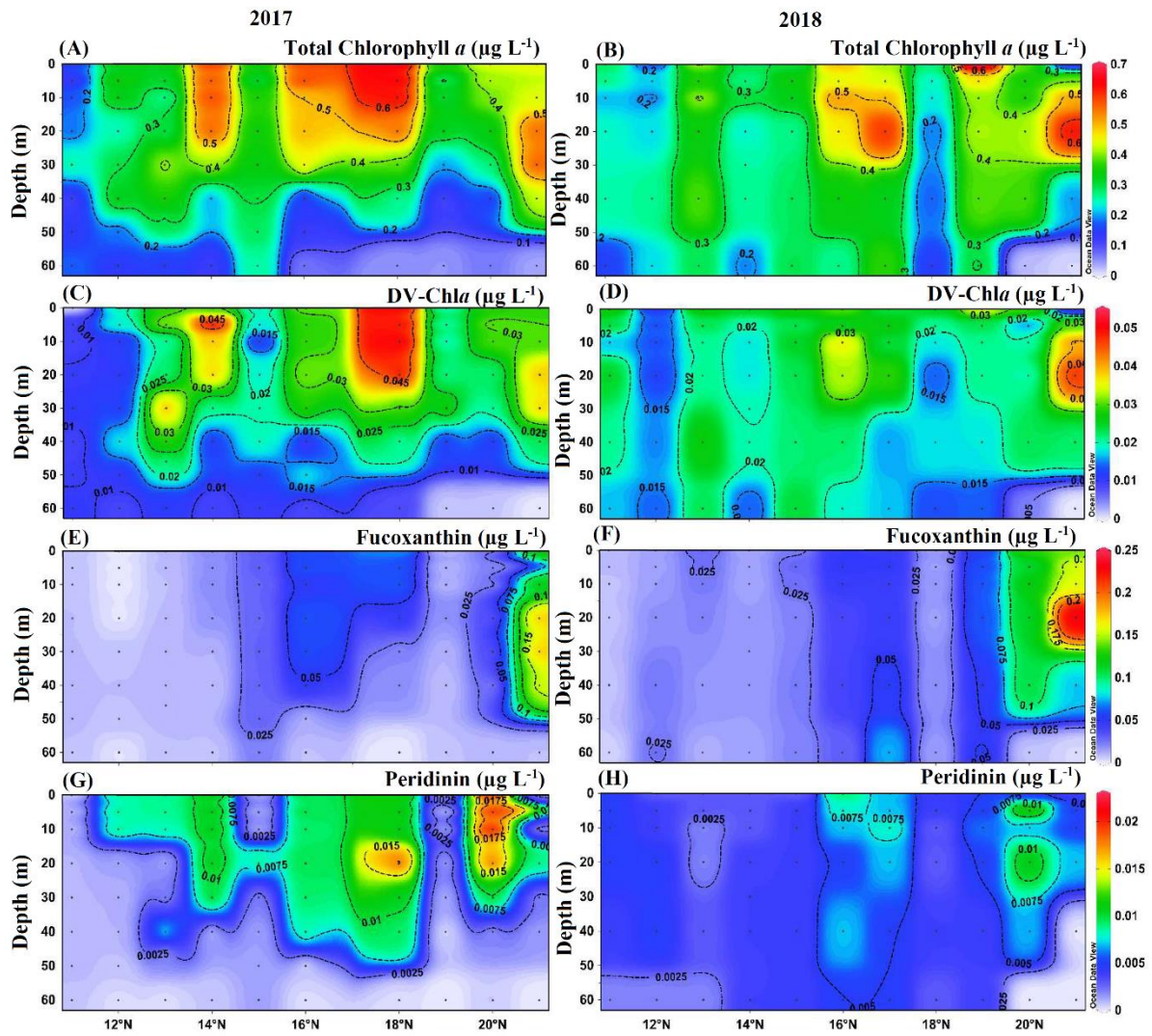


Figure 4 Latitudinal distributions of the concentrations of TChla (A, B), DV-Chla (C, D), fucoxanthin (E, F), and peridinin (G, H) during the summer monsoon 2017 (left panel) and 2018 (right panel) in the central Arabian Sea.

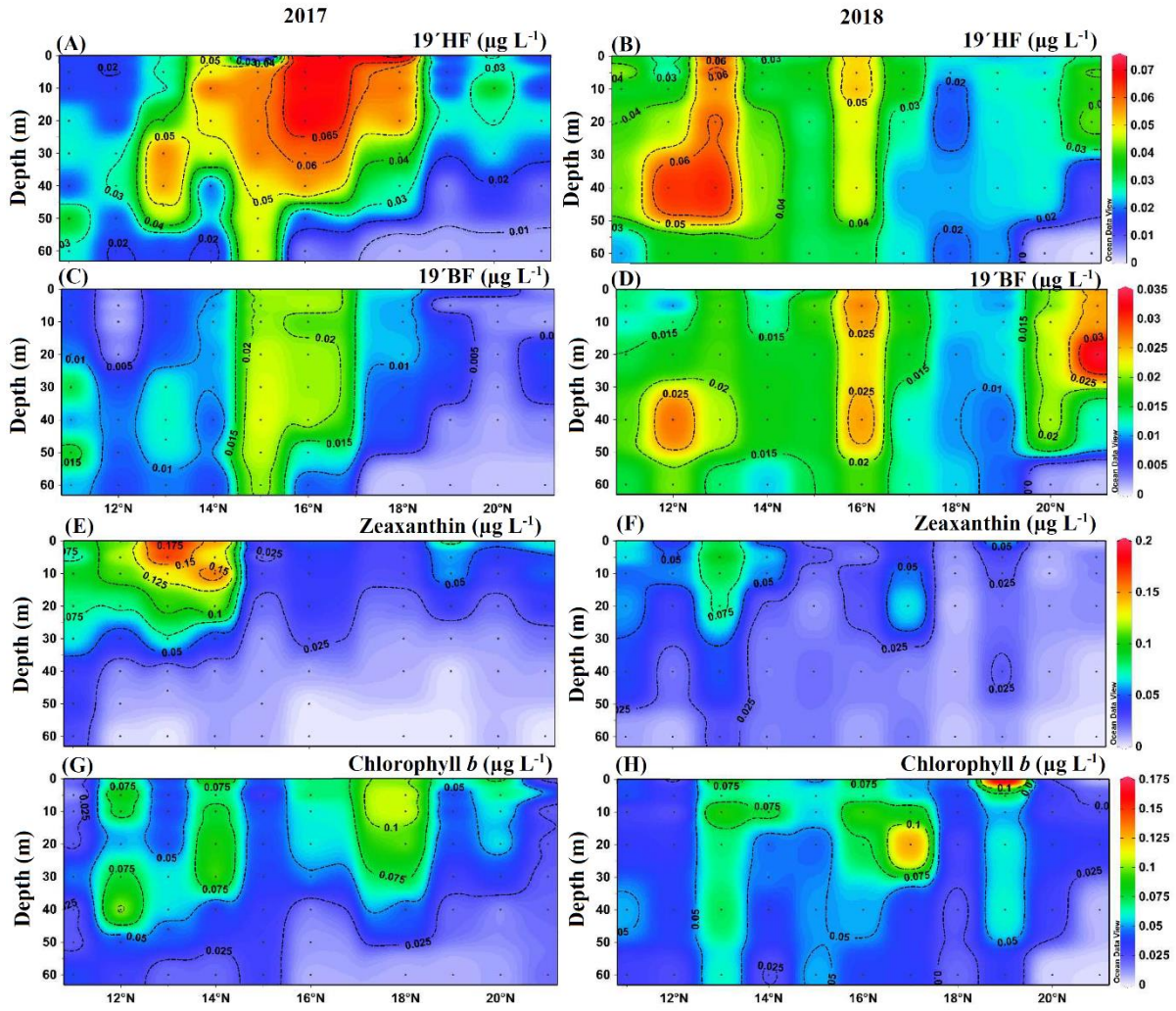


Figure 5 Latitudinal distributions of the concentrations of 19'HF (A, B), 19'BF (C, D), zeaxanthin (E, F), and chlorophyll *b* (G, H) during the summer monsoon 2017 and 2018 in the central Arabian Sea.

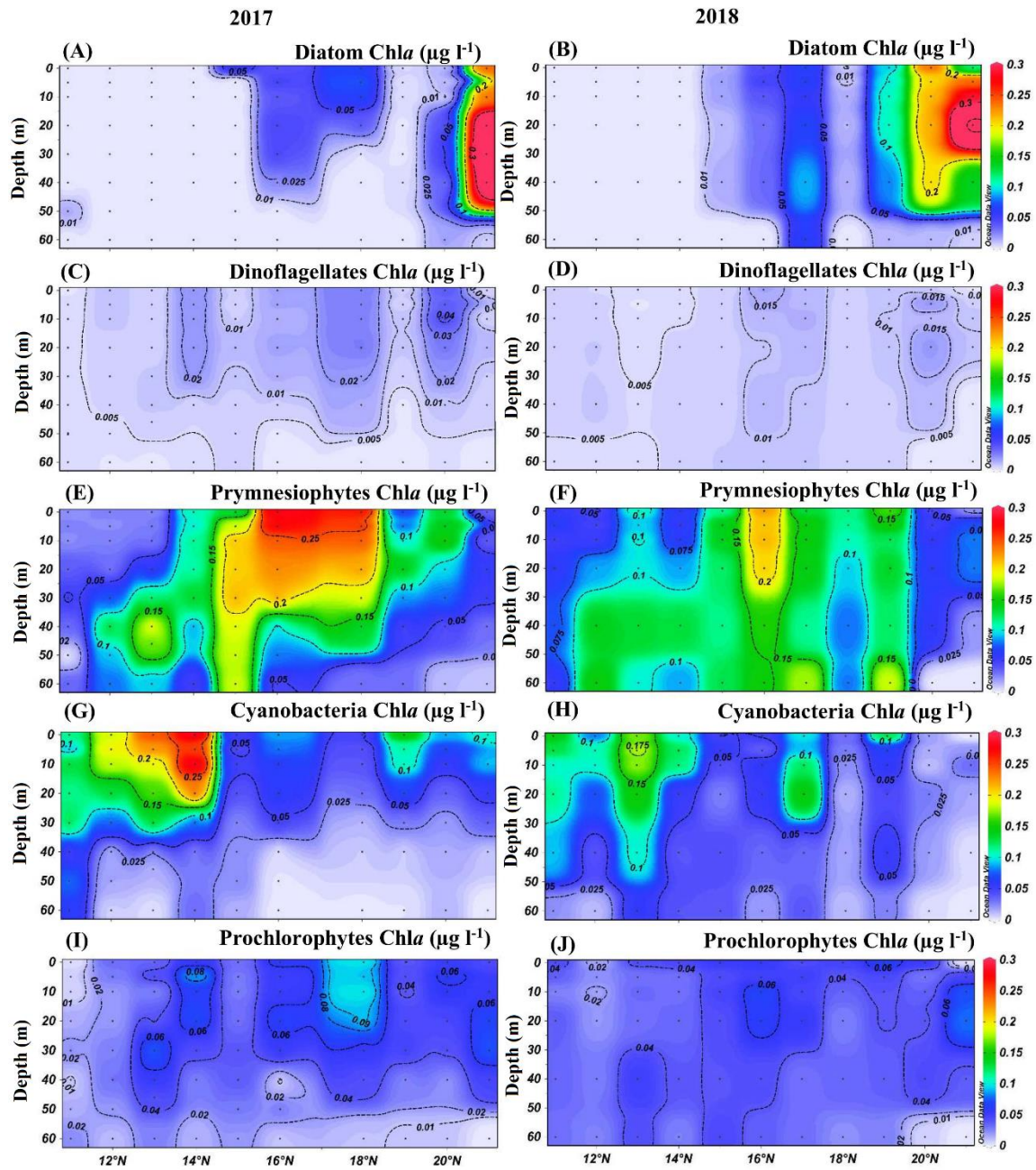


Figure 6 Cross-sectional profile of the relative percentage contributions of the major phytoplankton groups Diatoms (A, B), Dinoflagellates (C, D), Prymnesiophytes (E, F), Cyanobacteria (G, H), and Prochlorophytes (I, J) to total chlorophyll *a* estimated by the CHEMTAX program using marker pigments during the summer monsoon 2017 (left panel) and 2018 (right panel) in the central Arabian Sea.

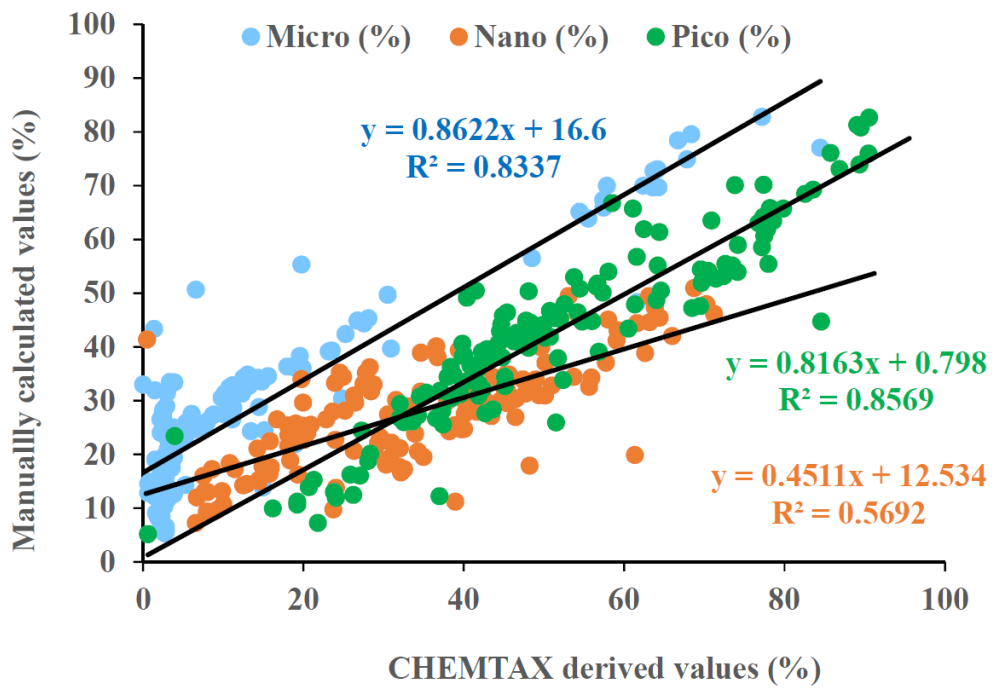


Figure 7 Correlations between the set of values of different size classes of phytoplankton manually derived and CHEMTAX analysis highlighting the significant linearity ($p < 0.0001$, $n = 140$).

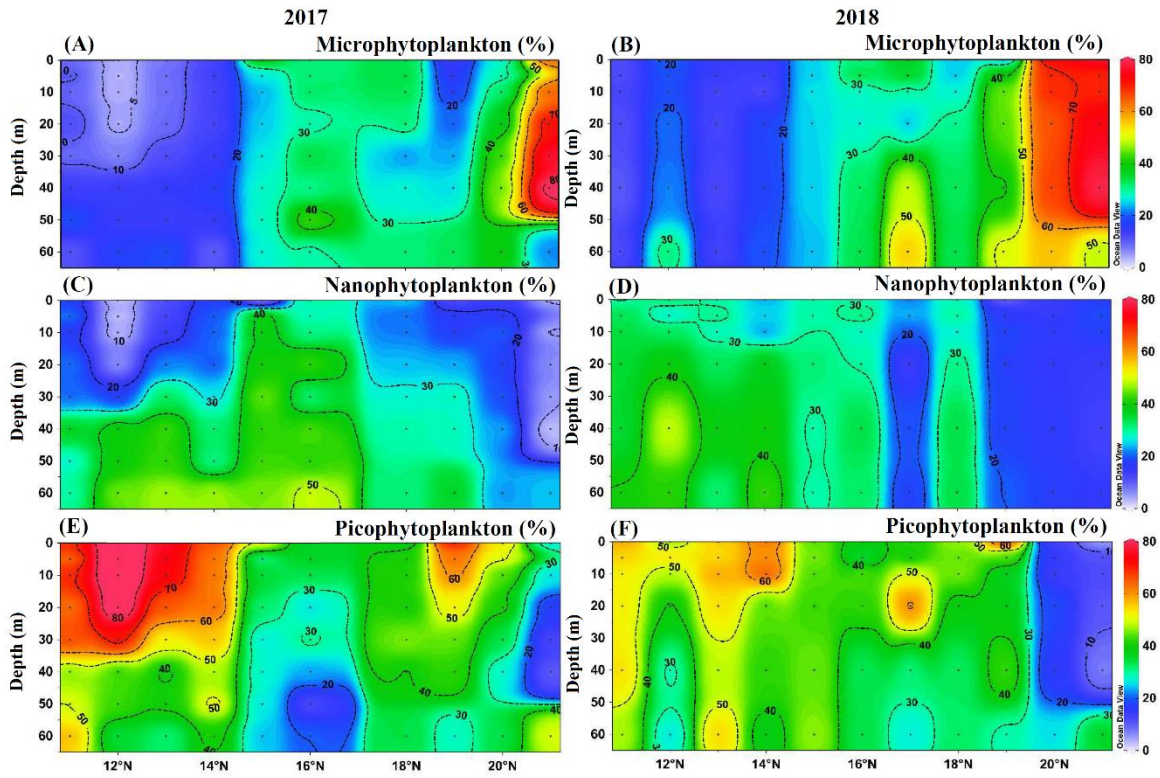


Figure 8 Cross-sectional profiles of different size classes of phytoplankton showing microphytoplankton (A, B), nanophytoplankton (C, D), and picophytoplankton (E, F) during the summer monsoon 2017 and 2018 in the central Arabian Sea.

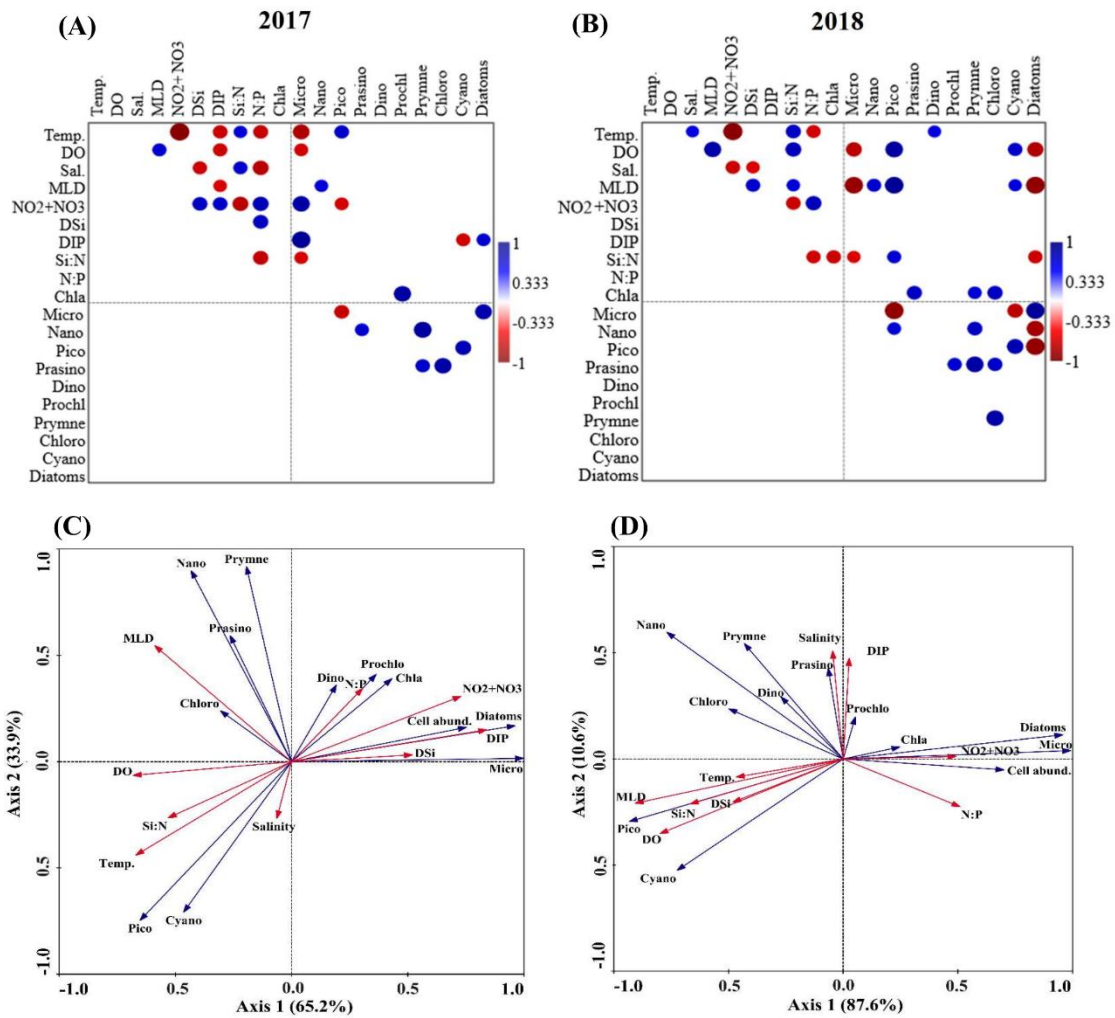
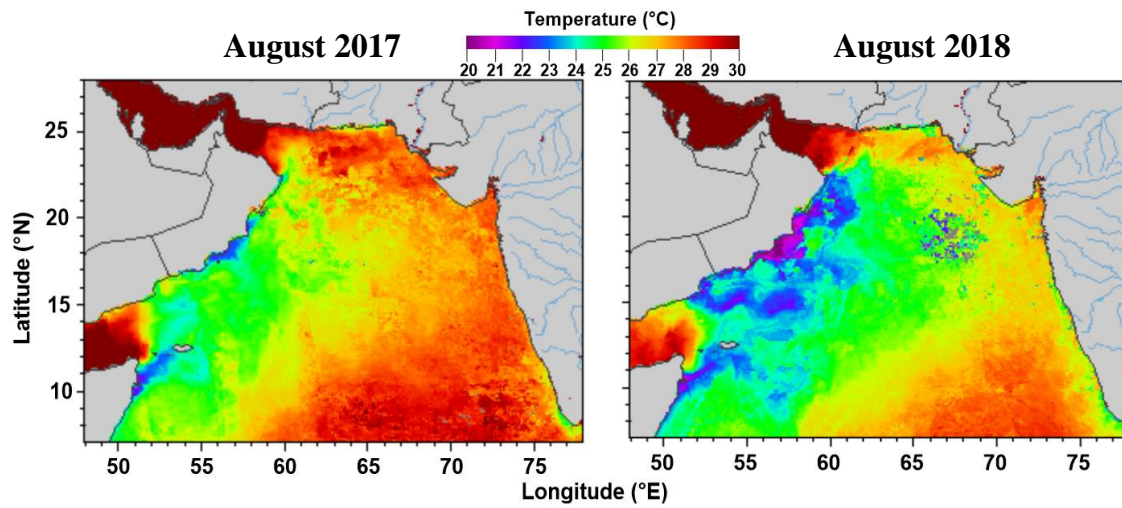


Figure 9 Correlation matrix between physicochemical parameters and phytoplankton major groups as well as size classes of (A) 2017 and (B) 2018. Only significant correlations ($p < 0.05$) are presented here and the correlation values ranged between -1 (dark red) to +1 (dark blue). RDA biplot showing the interrelationship between physicochemical parameters (red arrow) and phytoplankton size classes and major groups (blue arrow) during (C) 2017 and (D) 2018. Phytoplankton cell abundance (cell abund.) of microscopic analysis from Chowdhury et al. (2021) has been considered to validate the microphytoplankton contribution. Abbreviations: Temp: temperature; DO: dissolved oxygen; Sal: salinity; MLD: mixed layer depth; NO₂+NO₃: nitrate+nitrite; DSi: dissolved inorganic silicate; DIP: dissolved inorganic phosphate; Chla: Chlorophyll *a*; Micro: microphytoplankton; Nano: nanophytoplankton.

Supplementary Information

Figure S1: Latitudinal distribution of satellite derived monthly averaged sea surface temperature map obtained from the ERDDAP server (<https://coastwatch.pfeg.noaa.gov/erddap/index.html>)



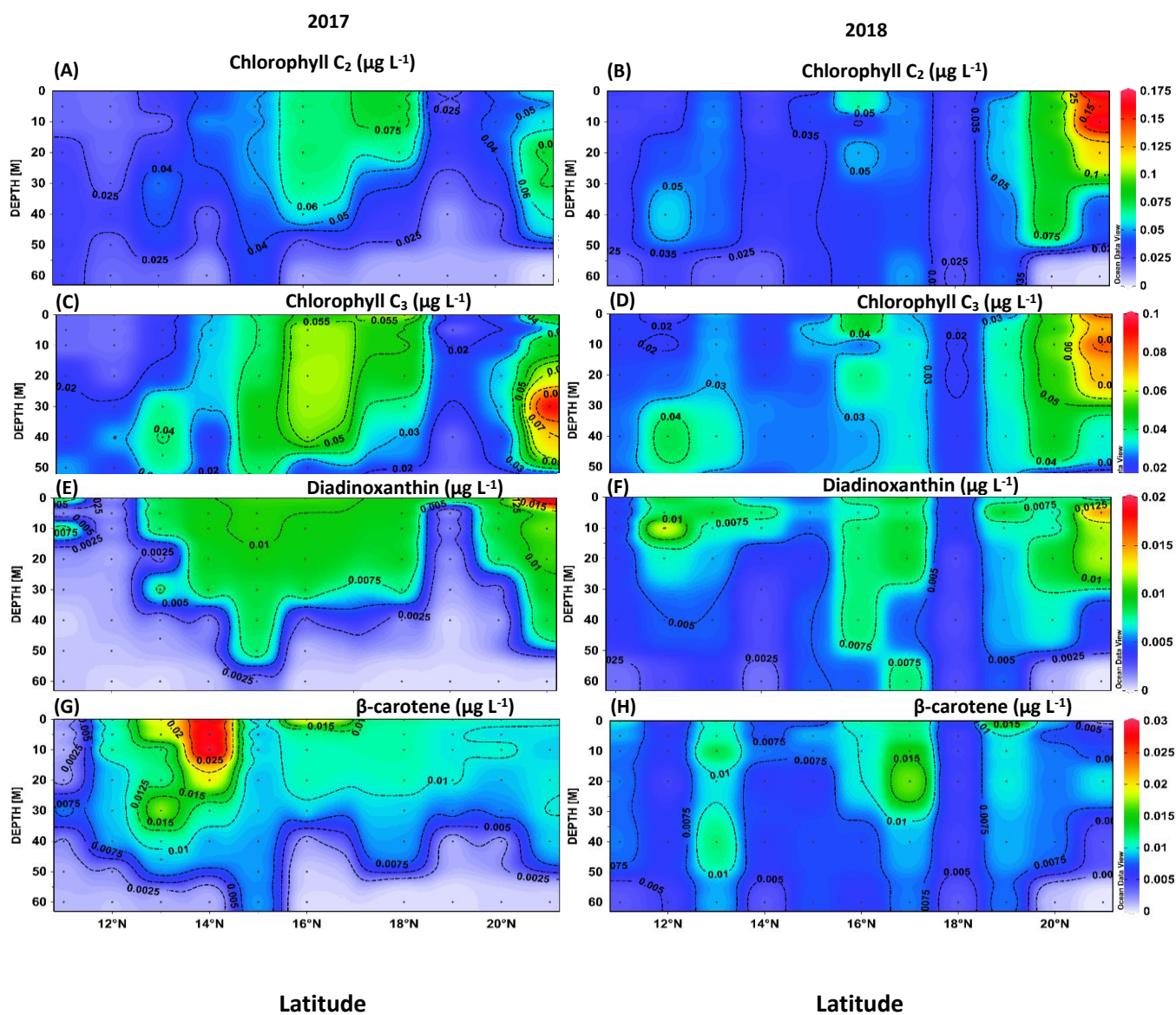


Figure S2: Cross-sectional profile of accessory pigments (A and B) chlorophyll c_2 , (C and D) chlorophyll c_3 , (E and F) diadinoxanthin and (G and H) β - carotene during the summer monsoon 2017 (left panel) and 2018 (right panel) in the central Arabian Sea.

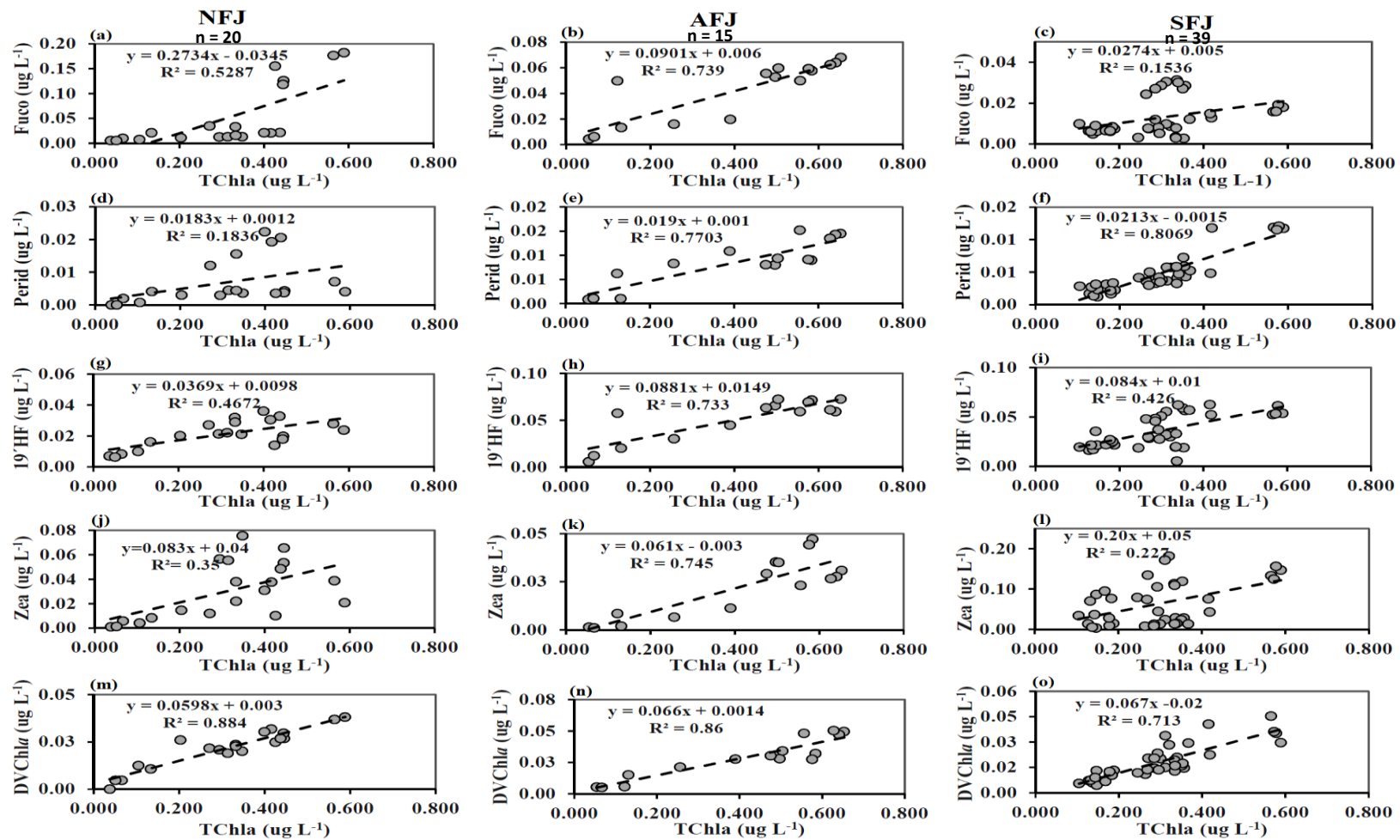


Figure S3 The figure showing the correlations between Tchl a and Fuco (a-c), Tchl a and Perid (d-f), Tchl a and 19' HF (g-i), Tchl a and Zea(j-l) and Tchl a and DV-Chl a(m-o) in the north of the Findlater Jet (NFJ), axis of the Findlater Jet (AFJ) and south of the Findlater Jet (SFJ), respectively during Aug 2017.

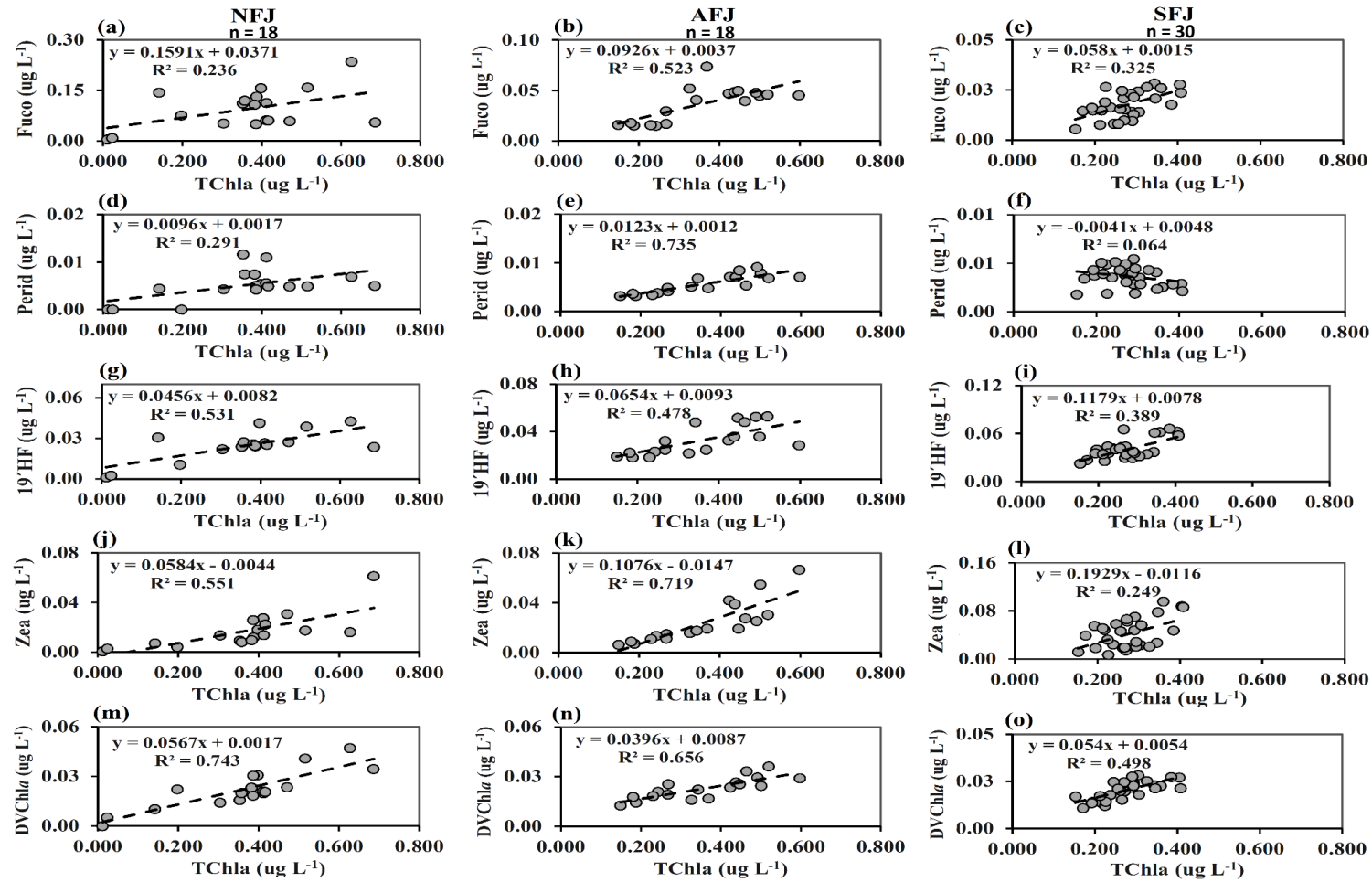


Figure S4 The figure showing correlation between (a-c)Tchl*a* and Fuco, (d-f) Tchl*a* and Perid, (g-i) Tchl*a* and 19' HF, (j-l) Tchl*a* and Zea and (m-o) Tchl*a* and DV-Chl*a* in the north of the Findlater Jet (NFJ), axis of the Findlater Jet (AFJ) and south of the Findlater Jet (SFJ), respectively during Aug 2018.

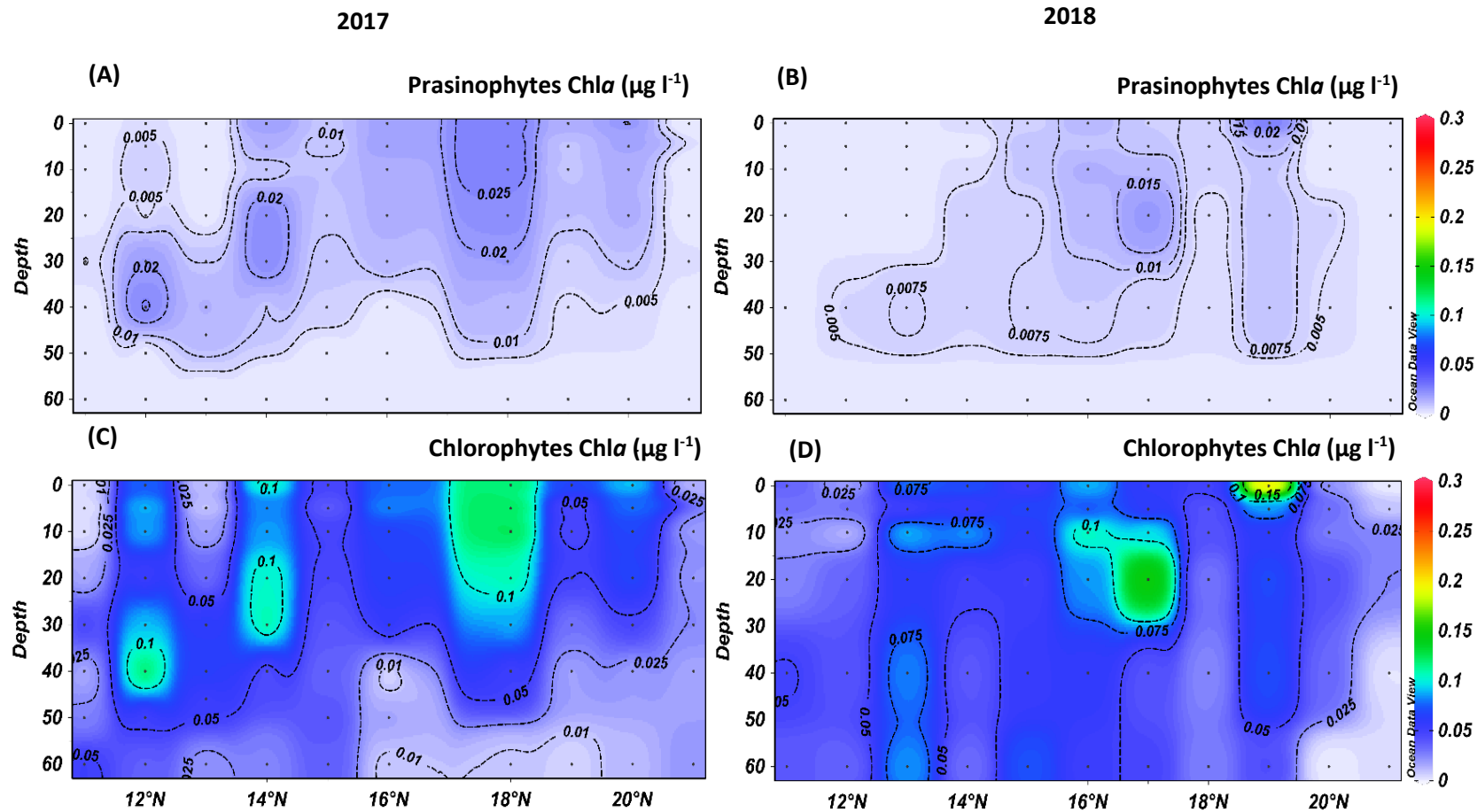


Figure S5 The relative contributions of prasinophytes in 2017 (A); 2018 (B), and the relative contributions of chlorophytes in 2017 (C) and 2018 (D) along the central Arabian Sea.

Table S1 Details of pigments and their abbreviations used in this study, their taxonomic/biogeochemical significance, and different size classes [modified from Vidussi et al. 2001; Uitz et al. 2006, Barlow et al. 2007].

Pigment	Abbreviation	Taxonomic or biogeochemical significance	Size class
Fucoxanthin	Fuco	Diatoms, prymnesiophytes, chrysophytes	Microphytoplankton
Peridinin	Perid	Dinoflagellates	Microphytoplankton
19' hexanoyloxyfucoxanthin	19' HF	Prymnesiophytes	Nanophytoplankton
19' butanoyloxyfucoxanthin	19' BF	Chrysophytes, prymnesiophytes	Nanophytoplankton
Chlorophyll <i>b</i>	Chl <i>b</i>	Chlorophytes, prasinophytes	Picophytoplankton
Zeaxanthin	Zea	Cyanobacteria, Prochlorophytes	Picophytoplankton
Divinyl Chlorophyll <i>a+b</i>	DV-Chl <i>a</i>	Prochlorophytes	Picophytoplankton

Table S2: Marker pigments to Chl *a* ratios for CHEMTAX analysis for two sampling periods (2017-2018). Input ratios were obtained from Roy et al. 2015.

Input matrix	Perid	19' BF	Fuco	19' HF	Neo	Prasino	Viola	DVChla	Lutein	Zea	Chl b	Chl a
Prasinophytes	0	0	0	0	0.061	0.127	0.025	0	0.004	0	0.381	1
Dinoflagellates	1.06	0	0	0	0	0	0	0	0	0	0	1
Prochlorophytes	0	0	0	0	0	0	0	0.418	0	0	0	1
Prymnesiophytes	0	0.02	1.21	1.36	0	0	0	0	0	0	0	1
Chlorophytes	0	0	0	0	0.04	0	0.1	0	0.127	0.12	0.57	1
Cyanobacteria	0	0	0	0	0	0	0	0	0	0.59	0	1
Diatoms	0	0	0.76	0	0	0	0	0	0	0	0	1
Output matrix (2017)												
Prasinophytes	0	0	0	0	0.028	0.058	0.011	0	0.002	0	0.173	1
Dinoflagellates	0.340	0	0	0	0	0	0	0	0	0	0	1
Prochlorophytes	0	0	0	0	0	0	0	0.331	0	0	0	1
Prymnesiophytes	0	0.004	0.137	0.263	0	0	0	0	0	0	0	1
Chlorophytes	0	0	0	0	0.012	0	0.030	0	0.038	0.036	0.302	1
Cyanobacteria	0	0	0	0	0	0	0	0	0	0.321	0	1
Diatoms	0	0	0.302	0	0	0	0	0	0	0	0	1
Output matrix (2018)												
Prasinophytes	0	0	0	0	0.028	0.058	0.011	0	0.002	0	0.173	1
Dinoflagellates	0.340	0	0	0	0	0	0	0	0	0	0	1
Prochlorophytes	0	0	0	0	0	0	0	0.331	0	0	0	1
Prymnesiophytes	0	0.004	0.137	0.263	0	0	0	0	0	0	0	1
Chlorophytes	0	0	0	0	0.012	0	0.029	0	0.033	0.035	0.322	1
Cyanobacteria	0	0	0	0	0	0	0	0	0	0.271	0	1
Diatoms	0	0	0.302	0	0	0	0	0	0	0	0	1

Table S3 The slopes of the equations, correlation coefficients (R^2), and the numbers of samples (n) between different pigments with total Chlorophyll a (TChla) in the north of the Findlater Jet (NFJ), the axis of the Findlater Jet (AFJ) and south of the Findlater Jet (SFJ) during 2017 and 2018. Statistically significant ($p < 0.05$) coefficient values (R^2) are marked in **bold**.

2017	NFJ			AFJ			SFJ		
	Slope	R^2	n	Slope	R^2	n	Slope	R^2	n
Fuco vs Tchla	0.273	0.53	20	0.090	0.74	15	0.027	0.15	39
Perid vs Tchla	0.018	0.18	20	0.019	0.77	15	0.021	0.81	39
19'HF vs Tchla	0.037	0.47	20	0.088	0.73	15	0.084	0.43	39
Zea vs Tchla	0.083	0.35	20	0.061	0.75	15	0.20	0.23	39
DV-Chla vs Tchla	0.06	0.88	20	0.066	0.86	15	0.067	0.73	39
2018									
Fuco vs Tchla	0.159	0.24	18	0.093	0.52	18	0.058	0.33	30
Perid vs Tchla	0.010	0.29	18	0.012	0.74	18	0.004	0.06	30
19'HF vs Tchla	0.046	0.53	18	0.065	0.48	18	0.118	0.39	30
Zea vs Tchla	0.058	0.55	18	0.108	0.72	18	0.193	0.25	30
DV-Chla vs Tchla	0.057	0.74	18	0.040	0.66	18	0.054	0.50	30